

**Parity-violating interaction effects in the  $np$  system**

R. Schiavilla

*Jefferson Lab, Newport News, Virginia 23606, USA**and Department of Physics, Old Dominion University, Norfolk, Virginia 23529, USA*

J. Carlson and M. Paris

*Theoretical Division, Los Alamos National Laboratory, Los Alamos, New Mexico 87545, USA*

(Received 29 April 2004; published 29 October 2004)

We investigate parity-violating observables in the  $np$  system, including the longitudinal asymmetry and neutron-spin rotation in  $\vec{n}p$  elastic scattering, the photon asymmetry in  $\vec{n}p$  radiative capture, and the asymmetries in deuteron photodisintegration  $d(\vec{\gamma}, n)p$  in the threshold region and electrodisintegration  $d(\vec{e}, e')np$  in quasielastic kinematics. To have an estimate of the model dependence for the various predictions, a number of different, latest-generation strong-interaction potentials—Argonne  $v_{18}$ , Bonn 2000, and Nijmegen I—are used in combination with a weak-interaction potential consisting of  $\pi$ -,  $\rho$ -, and  $\omega$ -meson exchanges—the Desplanques-Donoghue-Holstein (DDH) model. The complete bound and scattering problems in the presence of parity-conserving, including electromagnetic, and parity-violating potentials are solved in both configuration and momentum space. The issue of electromagnetic current conservation is examined carefully. We find large cancellations between the asymmetries induced by the parity-violating interactions and those arising from the associated pion-exchange currents. In the  $\vec{n}p$  capture, the model dependence is nevertheless quite small, because of constraints arising through the Siegert evaluation of the relevant  $E_1$  matrix elements. In quasielastic electron scattering these processes are found to be insignificant compared to the asymmetry produced by  $\gamma$ - $Z$  interference on individual nucleons. These two experiments, then, provide clean probes of different aspects of weak-interaction physics associated with parity violation in the  $np$  system. Finally, we find that the neutron-spin rotation in  $\vec{n}p$  elastic scattering and asymmetry in deuteron disintegration by circularly polarized photons exhibit significant sensitivity both to the values used for the weak vector-meson couplings in the DDH model and to the input strong-interaction potential adopted in the calculation. This reinforces the conclusion that these short-ranged meson couplings are not in themselves physical observables; rather, the parity-violating mixings are the physically relevant parameters.

DOI: 10.1103/PhysRevC.70.044007

PACS number(s): 13.75.Cs, 24.80.+y, 25.40.Cm

**I. INTRODUCTION**

A new generation of experiments have recently been completed, or are presently under way or in their planning phase, to study the effects of parity-violating (PV) interactions in  $pp$  elastic scattering [1],  $np$  radiative capture [2], and deuteron electrodisintegration [3] at low energies. There is also considerable interest in determining the extent to which hadronic weak interactions can affect the longitudinal asymmetry measured by the SAMPLE Collaboration in quasielastic scattering of polarized electrons off the deuteron [4], and therefore influence the extraction from these data (and those on the proton [5]) of the nucleon's strange magnetic and axial-vector form factors at four-momentum transfers squared of 0.04 and 0.09 (GeV/ $c$ )<sup>2</sup>.

The present is the third in a series of papers dealing with the theoretical investigation of PV interaction effects in two-nucleon systems. The first [6] was devoted to  $\vec{p}p$  elastic scattering, and presented a calculation of the longitudinal asymmetry induced by PV interactions in the lab-energy range 0–350 MeV. The second [7] provided a rather cursory account of a study of the PV asymmetries in  $\vec{n}p$  radiative capture at thermal neutron energies and in deuteron electrodisintegration at quasielastic kinematics. This work further extends that of Ref. [7] by investigating the neutron-spin

rotation at zero energy and the longitudinal asymmetry in  $\vec{n}p$  elastic scattering at lab energies between 0 and 350 MeV, and the photon-helicity dependence of the  $d(\vec{\gamma}, n)p$  cross section from threshold up to energies of 20 MeV. It also provides a thorough analysis of the results already presented in Ref. [7].

We adopt the PV potential developed by Desplanques, Donoghue, and Holstein [8] over 20 years ago, the so-called DDH model. In the  $np$  sector, it is conveniently parametrized in terms of  $\pi$ -,  $\rho$ -, and  $\omega$ -meson exchanges. In Ref. [8] the pion and vector-meson weak-coupling constants were estimated within a quark model approach incorporating symmetry techniques like  $SU(6)_W$  and current algebra requirements. Due to limitations inherent to such an analysis, however, the coupling constants so determined had rather wide ranges of allowed values.

Our prime motivations are to develop a systematic and consistent framework for studying PV observables in the few-nucleon systems, where accurate microscopic calculations are feasible, and to use available and forthcoming experimental data on these observables to constrain the strengths of the short- and long-range parts of the two-nucleon weak interaction. Indeed, in Ref. [6] we showed, for the case of the longitudinal asymmetry measured in  $\vec{p}p$  elastic scattering, how available experimental data provide

strong constraints on allowable combinations of  $\rho$ - and  $\omega$ -meson weak-coupling constants.

The remainder of the present paper is organized as follows. In Sec. II the PV potential as well as the parity-conserving strong-interaction potentials used in this work are briefly discussed, while in Sec. III the model for the nuclear electroweak currents is described, including the electromagnetic two-body terms induced by the presence of PV interactions. In Sec. IV a self-consistent treatment of the  $np$  bound- and scattering-state problems in both configuration and momentum spaces is provided, patterned after that of Ref. [6], and in Sec. V explicit expressions are derived for the longitudinal asymmetry and spin rotation in  $\vec{n}p$  elastic scattering, the photon asymmetry in  $\vec{n}p$  radiative capture, and the asymmetries in deuteron photo- and electrodisintegration. In Sec. VI the techniques used to calculate the PV observables are briefly reviewed, while in Sec. VII a fairly detailed analysis of the results is offered. Finally, Sec. VIII contains some concluding remarks.

## II. PARITY-CONSERVING AND PARITY-VIOLATING POTENTIALS

The parity-conserving (PC), strong-interaction potentials used in the present work are the Argonne  $v_{18}$  (AV18) [9], Nijmegen I (NIJM-I) [10], and CD-Bonn (BONN) [11] models. They were discussed in Ref. [6] in connection with the calculation of the longitudinal asymmetry in  $\vec{p}p$  elastic scattering. Here, we briefly summarize a few salient points.

These realistic potentials consist of a long-range part due to one-pion exchange and a short-range part modeled by one-boson exchange in the Bonn and Nijmegen, or parametrized in terms of functions of two-pion range or shorter in the AV18. They differ, however, in the treatment of the nonlocalities; the AV18 is local while the BONN and Nijmegen I have strong nonlocalities; these nonlocalities are of pion range in the case of the CD-Bonn.

The AV18 and NIJM-I potentials were fitted to the Nijmegen database of 1992 [12,13], consisting of 1787  $pp$  and 2514  $np$  scattering data, and both produced  $\chi^2$  per datum close to 1. The latest version of the charge-dependent Bonn potential, however, has been fitted to the 1999 database, consisting of 2932  $pp$  and 3058  $np$  data, for which it gives  $\chi^2$  per datum of 1.01 and 1.02, respectively [11]. The substantial increase in the number of  $pp$  data is due to the development of novel experimental techniques—internally polarized gas targets and stored, cooled beams. Indeed, using this technology, IUCF has produced a large number of  $pp$  spin-correlation parameters of very high precision; see, for example, Ref. [14]. It is worth noting that the AV18 potential, as an example, fits the post-1992 and both pre- and post-1992  $pp(np)$  data with  $\chi^2$ 's of 1.74 (1.02) and 1.35 (1.07), respectively [11]. Therefore, while the quality of their fits (to the  $pp$  data) has deteriorated somewhat in regard to the extended 1999 database, the AV18 and NIJM-I models can still be considered “realistic.”

As already mentioned in Sec. I, the form of the parity-violating weak-interaction potential was derived in Ref. [8]—the DDH model. In the isospin space of the  $np$  pair it is expressed as

TABLE I. Values used for the strong- and weak-interaction coupling constants and short-range cutoff parameters of the  $\pi$ ,  $\rho$ , and  $\omega$  meson to the nucleon in the DDH-adj potential.

	$g_\alpha^2/4\pi$	$\kappa_\alpha$	$10^7 \times h_\alpha^0$	$10^7 \times h_\alpha^1$	$10^7 \times h_\alpha^2$	$\Lambda_\alpha(\text{GeV}/c)$
$\pi$	13.9			4.56		1.72
$\rho$	0.84	6.1	-16.4	-2.77	-13.7	1.31
$\omega$	20	0	3.23	1.94		1.50

$$v_{T',T}^{\text{PV}} = \langle T', M_{T'}' = 0 | v^{\text{PV}} | T, M_T = 0 \rangle, \quad (2.1)$$

where  $T, T' = 0$  or  $1$ . The diagonal and off-diagonal terms are then obtained as

$$v_{T,T}^{\text{PV}} = \sum_{\alpha=\rho,\omega} -\frac{g_\alpha h_\alpha^{np}}{4\pi} \frac{m_\alpha}{m} (m_\alpha(1 + \kappa_\alpha) Y'(m_\alpha r) (\sigma_1 \times \sigma_2) \cdot \hat{\mathbf{r}} + (\sigma_1 - \sigma_2) \cdot [\mathbf{p}, Y(m_\alpha r)]_+), \quad (2.2)$$

$$v_{1,0}^{\text{PV}} = -i \frac{g_\pi h_\pi}{4\pi\sqrt{2}} \frac{m_\pi^2}{m} Y'(m_\pi r) (\sigma_1 + \sigma_2) \cdot \hat{\mathbf{r}} - \frac{g_\omega h_\omega^1 - g_\rho h_\rho^1}{4\pi} \frac{m_\rho}{m} \times (\sigma_1 + \sigma_2) \cdot [\mathbf{p}, Y(m_\rho r)]_+, \quad (2.3)$$

and  $v_{0,1}^{\text{PV}} = v_{1,0}^{\text{PV}\dagger}$ . In the equations above the relative position and momentum are defined as  $\mathbf{r} = \mathbf{r}_1 - \mathbf{r}_2$  and  $\mathbf{p} = (\mathbf{p}_1 - \mathbf{p}_2)/2$ , respectively,  $[\dots]_+$  denotes the anticommutator, and  $m, m_\pi, m_\rho$ , and  $m_\omega$  are the proton, pion,  $\rho$ -meson, and  $\omega$ -meson masses, respectively. The Yukawa function  $Y(x_\alpha)$ , suitably modified by the inclusion of monopole form factors, is given by

$$Y(x_\alpha) = \frac{1}{x_\alpha} \left\{ e^{-x_\alpha} - e^{-(\Lambda_\alpha/m_\alpha)x_\alpha} \left[ 1 + \frac{1}{2} \frac{\Lambda_\alpha}{m_\alpha} \left( 1 - \frac{m_\alpha^2}{\Lambda_\alpha^2} \right) x_\alpha \right] \right\}, \quad (2.4)$$

where  $x_\alpha \equiv m_\alpha r$ . Note that  $Y'(x)$  denotes  $dY(x)/dx$ , and that the terms proportional to  $Y'(x)$  in Eqs. (2.2) and (2.3) are usually written in the form of a commutator, since

$$i[\mathbf{p}, Y(m_\alpha r)]_- = m_\alpha Y'(m_\alpha r) \hat{\mathbf{r}}. \quad (2.5)$$

Finally, the values for the strong-interaction  $\pi$ -meson pseudoscalar coupling constant  $g_\pi$ , and  $\rho$ - and  $\omega$ -meson vector and tensor coupling constants  $g_\alpha$  and  $\kappa_\alpha$ , as well as for the cutoff parameters  $\Lambda_\alpha$ , are taken from the BONN model [11], and are listed in Table I. The weak-interaction vector-meson coupling constants  $h_\rho^{np}$  and  $h_\omega^{np}$  correspond to the following combinations of DDH parameters:

$$h_\rho^{np} = (4T - 3)h_\rho^0 - \frac{2}{\sqrt{6}} T h_\rho^2, \quad (2.6)$$

$$h_\omega^{np} = h_\omega^0, \quad (2.7)$$

where  $T = 0, 1$ . The values for these and for  $h_\pi, h_\rho^1$ , and  $h_\omega^1$  are listed in Table I. Note that we have taken the linear combination of  $\rho$ - and  $\omega$ -meson weak-coupling constants corresponding to  $\vec{p}p$  elastic scattering from the earlier analysis [6]

TABLE II. Values used for the strong- and weak-interaction coupling constants and short-range cutoff parameters of the  $\pi$ ,  $\rho$ , and  $\omega$  meson to the nucleon in the DDH “best values” potential, labeled “DDH,” from Ref. [8].

	$g_\alpha^2/4\pi$	$\kappa_\alpha$	$10^7 \times h_\alpha^0$	$10^7 \times h_\alpha^1$	$10^7 \times h_\alpha^2$	$\Lambda_\alpha(\text{GeV}/c)$
$\pi$	13.9			4.56		2.4
$\rho$	0.84	3.7	-11.4	-0.19	-9.5	2.4
$\omega$	20	0	-1.90	-1.14		2.4

of these experiments. We denote the model with these values for the coupling constants as DDH-adj. The remaining couplings are the “best value” estimates, suggested in Ref. [8].

In order to study the sensitivity of the calculated PV observables to variations in the weak-coupling constants, we also consider in the present work a  $v^{\text{PV}}$  corresponding to the original “best value” estimates for these from Ref. [8]; see Table II. Calculations with these sets of couplings are simply denoted by DDH.

### III. ELECTROMAGNETIC AND NEUTRAL WEAK-CURRENT OPERATORS

The electromagnetic current and charge operators, respectively  $\mathbf{j}$  and  $\rho$ , are expanded into a sum of one- and two-body terms,

$$\mathbf{j}(\mathbf{q}) = \sum_i \mathbf{j}_i(\mathbf{q}) + \sum_{i<j} \mathbf{j}_{ij}(\mathbf{q}), \quad (3.1)$$

and similarly for  $\rho(\mathbf{q})$ . The one-body terms have the standard expressions obtained from a nonrelativistic reduction of the covariant single-nucleon current [15]. The two-body charge operators are those derived in Ref. [16]; they only enter in the calculation of the asymmetry in the deuteron electrodisintegration at quasielastic kinematics, and will not be discussed further here.

The two-body currents have terms associated with the parity-conserving and parity-violating components of the interaction, respectively,  $\mathbf{j}_{ij}^{\text{PC}}$  and  $\mathbf{j}_{ij}^{\text{PV}}$ . The operators  $\mathbf{j}_{ij}^{\text{PC}}$  were derived explicitly in Ref. [17], and a complete listing of those relative to the Argonne  $v_{18}$  interaction [9] has been given most recently in Ref. [15]. Only the two-body currents associated with  $\pi$  and  $\rho$  exchange are retained in the case of the Bonn [11] and Nijmegen-I [10] interactions.

In addition to these, the purely transverse two-body currents associated with the excitation of  $\Delta$  isobars and the  $\rho\pi\gamma$  and  $\omega\pi\gamma$  mechanisms are included in all calculations. Again explicit expressions for these operators can be found in Ref. [15]. Note, however, that the  $\Delta$ -isobar degrees of freedom are treated in perturbation theory rather than with the transition-correlation-operator method [18], and that only effects due to single- $\Delta$  excitation are considered, according to Eqs. (2.15) and (3.4) in Ref. [15].

Before moving on to a discussion of the PV currents, we briefly review, for later reference, the question of conservation of the electromagnetic current for the case of the AV18. As pointed out in Ref. [15], the currents from its  $v_6$  part

(specifically, its isospin-dependent central, spin-spin, and tensor components) are strictly conserved. In a one-boson-exchange model, which the AV18 is not, these interaction components arise from  $\pi$  and  $\rho$  exchange.

The currents from the AV18 momentum-dependent ( $p$ -dependent) components—the spin-orbit,  $\mathbf{L}^2$ , and quadratic-spin-orbit terms—are also included. In Ref. [19] and later papers, the currents from the spin-orbit term were derived by generalizing the procedure used to obtain the  $v_6$  currents. It was assumed that the isospin-independent (isospin-dependent) central and spin-orbit interactions were due to  $\sigma$  and  $\omega$  exchanges ( $\rho$  exchange), and the associated two-body currents were constructed by considering corresponding  $\bar{N}N$ -pair diagrams involving these meson exchanges. The currents from the  $\mathbf{L}^2$  and quadratic-spin-orbit interactions were obtained, instead, by minimal substitution [15,17].

The currents from the  $p$ -dependent interactions are strictly not conserved, as one can easily surmise by considering their commutator with the charge density operator. For example, in the case of the isospin-dependent  $\mathbf{L}^2$  and  $(\mathbf{L} \cdot \mathbf{S})^2$  interactions, this commutator requires the presence of currents with the isospin structure  $(\tau_i \times \tau_j)_z$ , which cannot be generated by minimal substitution [17].

We will return to this issue in Sec. VII B. Here, we only want to emphasize that the currents from the  $p$ -dependent terms in the AV18 are short ranged. Their contributions to isovector observables, such as, for example, the magnetic form factors of the trinucleons [20], are found to be numerically much smaller than those due to the leading  $v_6$  currents. These currents also lead to small, although non-negligible, corrections to isoscalar observables, such as the deuteron magnetic moment and  $B(q)$  structure function [21]. However, in the case of the PV asymmetry in the  $\bar{n}p$  radiative capture at thermal energies under consideration in the present study, they will turn out to play an important role (see Sec. VII B).

#### A. Parity-violating currents

The DDH PV interaction [8] is parametrized in terms of  $\pi$ -,  $\rho$ -, and  $\omega$ -meson exchanges. The meson-nucleon phenomenological Lagrangian densities have been given most recently in Ref. [22]. We adopt here the notation and conventions of that work, except that we use pseudovector coupling for the  $\pi NN$  interaction Lagrangian, i.e.,

$$L_{\pi NN}^{\text{PC}} = - \frac{f_\pi}{m_\pi} \bar{N} \gamma_5 \gamma_\mu \tau N \cdot \partial^\mu \pi, \quad (3.2)$$

with  $f_\pi/m_\pi = g_\pi/(2m)$ . The resulting  $\gamma\pi NN$  coupling is given by

$$L_{\gamma\pi NN}^{\text{PC}} = - e \frac{f_\pi}{m_\pi} \bar{N} \gamma_5 \gamma_\mu (\tau \times \pi)_z N A^\mu, \quad (3.3)$$

and the  $\gamma\pi NN$  current is then obtained from the Feynman amplitude in Fig. 1(a). The complete PV  $\pi$ -exchange current is derived from a nonrelativistic reduction of both amplitudes in Fig. 1, and to leading order reads

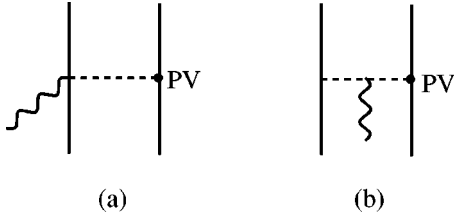


FIG. 1. Feynman diagram representation of the two-body currents associated with pion exchange: solid lines, nucleons; dashed lines, pions; wavy lines, photons. Note that one interaction vertex is parity conserving, while the other is parity violating (PV).

$$\mathbf{j}_{\pi,ij}^{\text{PV}}(\mathbf{k}_i, \mathbf{k}_j) = -\frac{f_\pi h_\pi}{\sqrt{2} m_\pi} (\tau_i \cdot \tau_j - \tau_{z,i} \tau_{z,j}) \left( v_\pi(k_j) \sigma_i + v_\pi(k_i) \sigma_j - \frac{\mathbf{k}_i - \mathbf{k}_j}{k_i^2 - k_j^2} [v_\pi(k_j) - v_\pi(k_i)] (\sigma_i \cdot \mathbf{k}_i - \sigma_j \cdot \mathbf{k}_j) \right), \quad (3.4)$$

where  $v_\pi(k)$  is defined as

$$v_\pi(k) = \left( \frac{\Lambda_\pi^2 - m_\pi^2}{k^2 + \Lambda_\pi^2} \right)^2 \frac{1}{k^2 + m_\pi^2}, \quad (3.5)$$

$\mathbf{k}_i = \mathbf{p}'_i - \mathbf{p}_i$  is the fractional momentum delivered to nucleon  $i$  (with these definitions  $\mathbf{q} = \mathbf{k}_i + \mathbf{k}_j$ ), and  $\Lambda_\pi$  is a short-range cutoff. In the limit of pointlike couplings, the current above is identical to that listed in Eqs. (A7a) and (A9a) of Ref. [22].  $N\bar{N}$ -pair terms arising from the photon coupling to the nucleon line containing a PV  $\pi NN$  vertex do not contribute to leading order. Lastly, we note that  $\mathbf{j}_\pi^{\text{PV}}$  satisfies current conservation with the PV  $\pi$ -exchange interaction, given in momentum space by

$$\mathbf{j}_\pi^{\text{PV}}(\mathbf{k}_i, \mathbf{k}_j) = -i \frac{f_\pi h_\pi}{\sqrt{2} m_\pi} (\tau_i \times \tau_j)_z v_\pi(k_j) \sigma_i \cdot \mathbf{k}_j + i \rightleftharpoons j, \quad (3.6)$$

since

$$\begin{aligned} & [v_\pi^{\text{PV}}(\mathbf{k}_i - \mathbf{q}, \mathbf{k}_j), P_i] + [v_\pi^{\text{PV}}(\mathbf{k}_i, \mathbf{k}_j - \mathbf{q}), P_j] \\ &= -\frac{f_\pi h_\pi}{\sqrt{2} m_\pi} (\tau_i \cdot \tau_j - \tau_{z,i} \tau_{z,j}) [v_\pi(k_i) (\sigma_i + \sigma_j) \cdot \mathbf{k}_i + i \rightleftharpoons j], \end{aligned} \quad (3.7)$$

which is easily seen to be the same as  $(\mathbf{k}_i + \mathbf{k}_j) \cdot \mathbf{j}_\pi^{\text{PV}}(\mathbf{k}_i, \mathbf{k}_j)$ . Here  $P_i$  denotes the isospin projection operator

$$P_i \equiv \frac{1 + \tau_{z,i}}{2}. \quad (3.8)$$

In the present work, the PV currents induced by  $\rho$ - and  $\omega$ -meson exchanges have been neglected, since, due their short-range character, the associated contributions are expected to be tiny. We note, however, that in Eq. (A5) of Ref. [22] a  $\gamma\rho NN$  contact term, originating from gauging the  $\rho NN$  tensor coupling, has been ignored, although it is included in a later paper [23] by one of the authors of Ref. [22]. This term is given by

$$L_{\gamma\rho NN} = e \frac{g_\rho \kappa_\rho}{2m} \bar{N} \sigma_{\mu\nu} (\boldsymbol{\tau} \times \boldsymbol{\rho}^\mu)_z N A^\nu, \quad (3.9)$$

and leads, in leading order, to an additional term in Eq. (A7c) of Ref. [22] of the form

$$\begin{aligned} & -\frac{g_\rho \kappa_\rho}{2m} \left( h_\rho^0 - \frac{h_\rho^2}{2\sqrt{6}} \right) (\tau_i \times \tau_j)_z v_\rho(k_j) \\ & \times \left[ \sigma_i \times \sigma_j + \frac{\boldsymbol{\sigma}_j \cdot \mathbf{k}_j}{m_\rho^2} \sigma_i \times \mathbf{k}_j \right] + i \rightleftharpoons j, \end{aligned} \quad (3.10)$$

with  $v_\rho(k)$  defined similarly as in Eq. (3.5). The term above, when combined with that having the same structure in the second line of Eq. (A7c) of Ref. [22], generates a contribution proportional to  $1 + \kappa_\rho$  which, in view of the large value of the  $\rho NN$  tensor coupling constant ( $\kappa_\rho = 6.6$ ), is expected to be dominant in the PV  $\rho$ -exchange current. The delicate issue of current conservation when vector-meson exchanges are included is not discussed in the present work.

Finally, there is a PV one-body current originating from the nucleon's anapole moment. It can be derived, for example, by considering pion-loop diagrams where one of the vertices involves a PV  $\pi NN$  coupling; it has the structure, to leading order, given by

$$\mathbf{j}_i^{\text{PV}}(\mathbf{q}) = -\frac{q_\mu^2}{2m^2} [a^S(q_\mu^2) + a^V(q_\mu^2) \tau_{z,i}] \sigma_i e^{i\mathbf{q} \cdot \mathbf{r}_i}, \quad (3.11)$$

where  $q_\mu^2$  is the four-momentum transfer,  $q_\mu^2 = \omega^2 - q^2$ , and the isoscalar and isovector anapole form factors are normalized as

$$a^{S,V}(0) = \frac{g_\pi h_\pi}{4\sqrt{2}\pi^2} \alpha^{S,V}, \quad (3.12)$$

with  $\alpha^S = 1.6$  and  $\alpha^V = 0.4$  from a calculation of pion-loop contributions [24]. More recent estimates of the nucleon anapole form factors predict [25–27] somewhat different values for  $\alpha^{S,V}$ . A complete treatment would require estimates of short-distance contributions [28] and electroweak radiative corrections. Thus, in view of the uncertainties in the quantitative estimate of these effects, we will continue to use the values above in the present study (see also Sec. VII D). Note that  $\mathbf{j}_i^{\text{PV}}$  vanishes for real-photon transitions.

## B. Neutral weak currents

In the standard model the vector part of the neutral weak current,  $j^{0,\sigma}$ , is related to the isoscalar (S) and isovector (V) components of the electromagnetic current, denoted, respectively, as  $j_S^{\gamma,\sigma}$  and  $j_V^{\gamma,\sigma}$ , via

$$j^{0,\sigma} = -2 \sin^2 \theta_W j_S^{\gamma,\sigma} + (1 - 2 \sin^2 \theta_W) j_V^{\gamma,\sigma}, \quad (3.13)$$

where  $\theta_W$  is the Weinberg angle, and therefore the associated one- and two-body weak charge and current operators are easily obtained from those given in Sec. III. The axial charge and current operators too have one- and two-body terms. Only the axial current

$$\mathbf{j}^5(\mathbf{q}) = \sum_i \mathbf{j}_i^5(\mathbf{q}) + \sum_{i<j} \mathbf{j}_{ij}^5(\mathbf{q}) \quad (3.14)$$

is needed in the present work. The one- and two-body operators are essentially those listed in Ref. [29], except for obvious changes in the isospin structure having to do with the fact that we are dealing here with neutral rather than charge-raising/lowering weak currents, and for the inclusion of nucleon and  $N\Delta$  axial form factors—the parametrization adopted for these is given in Ref. [30]. Note that in Ref. [32] the relativistic corrections in  $\mathbf{j}_i^5$  and two-body axial currents were neglected, in line with the expectation, confirmed in the present study, that the associated contributions were small.

Finally, the neutral weak currents given above are at tree level; electroweak radiative corrections as well as strange-quark contributions to the vector and axial-vector currents [31] have been ignored. These effects have been taken into account in recent calculations of the longitudinal asymmetry in  $d(\vec{e}, e')pn$  at quasielastic kinematics [33]; however, they will not be discussed further here.

#### IV. FORMALISM

In this section we discuss the  $np$  scattering- and bound-state problems in the presence of a potential  $v$  given by

$$v = v^{\text{PC}} + v^{\text{PV}}, \quad (4.1)$$

where  $v^{\text{PC}}$  and  $v^{\text{PV}}$  denote the parity-conserving and parity-violating components induced by the strong (including electromagnetic) and weak interactions, respectively. The formalism and notation are similar to those developed in Ref. [6].

##### A. Partial-wave expansions of scattering state and $T$ and $S$ matrices

The Lippmann-Schwinger equation for the  $NN$  scattering state  $|\mathbf{p}, SM_S, T\rangle^{(\pm)}$ , where  $\mathbf{p}$  is the relative momentum, and  $S, M_S, T$ , and  $M_T=0$  specify the pair spin, spin-projection, isospin, and isospin-projection states (note that the label  $M_T=0$  is unnecessary, since  $v$  is diagonal in  $M_T$ ), can be written as [34]

$$|\mathbf{p}, SM_S, T\rangle^{(\pm)} = |\mathbf{p}, SM_S, T\rangle_0 + \frac{1}{E - H_0 \pm i\epsilon} v |\mathbf{p}, SM_S, T\rangle^{(\pm)}, \quad (4.2)$$

where  $H_0$  is the free Hamiltonian, and  $|\dots\rangle_0$  are the eigenstates of  $H_0$ , namely, plane waves,

$$\begin{aligned} \phi_{\mathbf{p}, SM_S, T}(\mathbf{r}) &= \langle \mathbf{r} | \mathbf{p}, SM_S, T \rangle_0 \\ &= \frac{1}{\sqrt{2}} [e^{i\mathbf{p}\cdot\mathbf{r}} - (-)^{S+T} e^{-i\mathbf{p}\cdot\mathbf{r}}] \chi_{M_S}^S \eta_{M_T=0}^T \\ &= 4\pi\sqrt{2} \sum_{JM_JL} i^L \epsilon_{LST} j_L(pr) [Z_{LSM_S}^{JM_J}(\hat{\mathbf{p}})]^* \mathcal{Y}_{LSJ}^{M_J}(\hat{\mathbf{r}}) \eta_0^T. \end{aligned} \quad (4.3)$$

Here  $j_L(pr)$  denotes the regular spherical Bessel function,

and the following definitions have been introduced:

$$Z_{LSM_S}^{JM_J}(\hat{\mathbf{p}}) \equiv \sum_{M_L} \langle LM_L, SM_S | JM_J \rangle Y_{LM_L}(\hat{\mathbf{p}}), \quad (4.4)$$

$$\epsilon_{LST} \equiv \frac{1}{2} [1 - (-1)^{L+S+T}]. \quad (4.5)$$

The factor  $\epsilon_{LST}$  ensures that the plane waves are properly antisymmetrized.

The  $T$  matrix corresponding to the potential  $v$  is defined as [34]

$$T(\mathbf{p}', S' M'_S, T'; \mathbf{p}, SM_S, T) = \langle \mathbf{p}', S' M'_S, T' | v | \mathbf{p}, SM_S, T \rangle^{(+)}. \quad (4.6)$$

Insertion of the plane wave states  $|\mathbf{p}, SM_S, T\rangle_0$  into the right-hand side of the Lippmann-Schwinger equation leads to

$$\begin{aligned} |\mathbf{p}, SM_S, T\rangle^{(+)} &= |\mathbf{p}, SM_S, T\rangle_0 + \sum_{S' M'_S T'} \int \frac{d\mathbf{p}'}{(2\pi)^3} \frac{1}{2} \\ &\times |\mathbf{p}', S' M'_S, T'\rangle_0 \frac{T(\mathbf{p}', S' M'_S, T'; \mathbf{p}, SM_S, T)}{E - p'^2/(2\mu) + i\epsilon}, \end{aligned} \quad (4.7)$$

from which the partial-wave expansion of the scattering state is easily obtained by first noting that the potential, and hence the  $T$  matrix, can be expanded as

$$\begin{aligned} \langle \mathbf{p}', S' M'_S, T' | v | \mathbf{p}, SM_S, T \rangle_0 &= 2(4\pi)^2 \sum_{JM_J L L'} \epsilon_{L' S' T'} \epsilon_{LST} Z_{L' S' M'_S}^{JM_J}(\hat{\mathbf{p}}') \\ &\times [Z_{LSM_S}^{JM_J}(\hat{\mathbf{p}})]^* v_{L' S' T', LST}^J(p'; p), \end{aligned} \quad (4.8)$$

with

$$\begin{aligned} v_{L' S' T', LST}^J(p'; p) &= i^{L-L'} \int d\mathbf{r} j_{L'}(p'r) \mathcal{Y}_{L' S' J}^{M_J}(\hat{\mathbf{r}}) \eta_0^{T'\dagger} \\ &\times v(\mathbf{r}) \eta_0^T \mathcal{Y}_{LSJ}^{M_J}(\hat{\mathbf{r}}) j_L(pr). \end{aligned} \quad (4.9)$$

After insertion of the corresponding expansion for the  $T$  matrix into Eq. (4.7) and a number of standard manipulations, the scattering-state wave function can be written as

$$\begin{aligned} \psi_{\mathbf{p}, SM_S, T}^{(+)}(\mathbf{r}) &= 4\pi\sqrt{2} \sum_{JM_J L L' S' T'} i^{L'} \epsilon_{L' S' T'} \epsilon_{LST} [Z_{LSM_S}^{JM_J}(\hat{\mathbf{p}})]^* \\ &\times \frac{w_{L' S' T', LST}^J(r; p)}{r} \mathcal{Y}_{L' S' J}^{M_J}(\hat{\mathbf{r}}) \eta_0^{T'}, \end{aligned} \quad (4.10)$$

with

$$\begin{aligned} \frac{w_{\alpha', \alpha}^j(r; p)}{r} &= \delta_{\alpha', \alpha} j_{L'}(pr) + \frac{2}{\pi} \int_0^\infty dp' p'^2 j_{L'}(p'r) \\ &\times \frac{1}{E - p'^2/(2\mu) + i\epsilon} T_{\alpha', \alpha}^J(p'; p), \end{aligned} \quad (4.11)$$

where the label  $\alpha(\alpha')$  stands for the set of quantum numbers

TABLE III. Labeling of channels.

$J$	$\alpha$			
	1	2	3	4
0	$^1S_0$	$^3P_0$		
1	$^3S_1$	$^3D_1$	$^1P_1$	$^3P_1$
2	$^3P_2$	$^3F_2$	$^1D_2$	$^3D_2$
3	$^3D_3$	$^3G_3$	$^1F_3$	$^3F_3$
$\vdots$	$\vdots$	$\vdots$	$\vdots$	$\vdots$

$LST(L'S'T')$ . The (complex) radial wave function  $w(r)$  behaves in the asymptotic region  $r \rightarrow \infty$  as

$$\frac{w_{\alpha',\alpha}^J(r;p)}{r} \simeq \frac{1}{2} [\delta_{\alpha',\alpha} h_{L'}^{(2)}(pr) + h_{L'}^{(1)}(pr) S_{\alpha',\alpha}^J(p)], \quad (4.12)$$

where the on-shell ( $p'=p$ )  $S$  matrix has been introduced,

$$S_{\alpha',\alpha}^J(p) = \delta_{\alpha',\alpha} - 4i \mu p T_{\alpha',\alpha}^J(p;p), \quad (4.13)$$

and the functions  $h^{(1,2)}(pr)$  are defined in terms of the regular and irregular ( $n_L$ ) spherical Bessel functions as

$$h_L^{(1,2)}(pr) = j_L(pr) \pm i n_L(pr). \quad (4.14)$$

### B. Schrödinger equation, phase shifts, mixing angles, and the scattering amplitude

The coupled-channel Schrödinger equations for the radial wave functions  $w(r)$  read

$$\left( -\frac{d^2}{dr^2} + \frac{L'(L'+1)}{r^2} - p^2 \right) w_{\alpha',\alpha}^J(r;p) + \sum_{\beta} r v_{\alpha',\beta}^J(r) \frac{1}{r} w_{\beta,\alpha}^J(r;p) = 0, \quad (4.15)$$

with

$$v_{\alpha',\alpha}^J(r) = i^{L-L'} 2\mu \int d\Omega \mathcal{Y}_{\alpha'J}^{M_J \dagger} \eta_0^{T' \dagger} v(\mathbf{r}) \eta_0^T \mathcal{Y}_{\alpha J}^{M_J}, \quad (4.16)$$

where, because of time-reversal invariance, the matrix  $v_{\alpha',\alpha}^J$  can be shown to be real and symmetric [this is the reason for the somewhat unconventional phase factor in Eq. (4.16); in order to maintain symmetry for both the  $v^{\text{PC}}$  and  $v^{\text{PV}}$  matrices, and hence the  $S$  matrix, the states used here differ by a factor  $i^L$  from those usually used in nucleon-nucleon scattering analyses]. The asymptotic behavior of the  $w(r)$ 's is given in Eq. (4.12), while explicit expressions for the radial functions  $v_{\alpha',\alpha}^{J,\text{PV}}(r)$  can be found in Ref. [6]—those associated with  $v^{\text{PC}}$  are well known.

There are two coupled channels for  $J=0$ , and four coupled channels for  $J \geq 1$ . The situation is summarized in Table III. Again because of the invariance under time-

inversion transformations of  $v^{\text{PC}+v^{\text{PV}}}$ , the  $S$  matrix is symmetric (apart from also being unitary), and can therefore be written as [34]

$$S^J = U^T S_D^J U, \quad (4.17)$$

where  $U$  is a real orthogonal matrix, and  $S_D^J$  is a diagonal matrix of the form

$$S_{D,\alpha',\alpha}^J = \delta_{\alpha',\alpha} e^{2i\delta_{\alpha'}^J}. \quad (4.18)$$

Here  $\delta_{\alpha'}^J$  is the (real) phase shift in channel  $\alpha$ , which is a function of the energy  $E$  with  $p = \sqrt{2\mu E}$ . The mixing matrix  $U$  can be written as

$$U = U^{(12)}, \quad J=0, \quad (4.19)$$

$$= \prod_{1 \leq i < j \leq 4} U^{(ij)}, \quad J \geq 1, \quad (4.20)$$

where  $U^{(ij)}$  is the  $2 \times 2$  or  $4 \times 4$  orthogonal matrix that includes the coupling between channels  $i$  and  $j$  only, for example,

$$U^{(13)} = \begin{bmatrix} \cos \epsilon'_{13} & 0 & \sin \epsilon'_{13} & 0 \\ 0 & 1 & 0 & 0 \\ -\sin \epsilon'_{13} & 0 & \cos \epsilon'_{13} & 0 \\ 0 & 0 & 0 & 1 \end{bmatrix} \simeq 1 + \epsilon'_{13} \begin{bmatrix} 0 & 0 & 1 & 0 \\ 0 & 0 & 0 & 0 \\ -1 & 0 & 0 & 0 \\ 0 & 0 & 0 & 0 \end{bmatrix}.$$

Note that no coupling is allowed between channels 3 and 4 in the notation of Table III, and hence  $U^{(34)}=1$ . Thus, for  $J=0$  there are two phase shifts and a mixing angle, while for  $J \geq 1$  there are four phase shifts and five mixing angles. Of course, since  $|v^{\text{PV}}| \ll |v^{\text{PC}}|$ , the mixing angles  $\epsilon'_{ij}$  induced by  $v^{\text{PV}}$  are  $\ll 1$ , a fact already exploited in the last expression above for  $U$ . Given the channel ordering in Table III, Table IV specifies which of the channel mixings are induced by  $v^{\text{PC}}$  and which by  $v^{\text{PV}}$ .

The reality of the potential matrix elements  $v_{\alpha',\alpha}^J(r)$  makes it possible to construct real solutions of the Schrödinger equation (4.15). The problem is reduced to determining the relation between these solutions and the com-

$J$	Coupling				
	12	13	14	23	24
0	PV				
1	PC	PV	PV	PV	PV
2	PC	PV	PV	PV	PV
...	PC	PV	PV	PV	PV

plex  $w(r)$ 's functions. Using Eq. (4.17) and  $U^T U = 1$ , the  $w(r)$ 's can be expressed in the asymptotic region as

$$\begin{aligned} \frac{w_{\alpha',\alpha}^J}{r} &\simeq \sum_{\beta} (U^T)_{\alpha'\beta} e^{i\delta_{\beta}^J} \frac{h_{\alpha'}^{(2)} e^{-i\delta_{\beta}^J} + h_{\alpha'}^{(1)} e^{i\delta_{\beta}^J}}{2} U_{\beta\alpha} \\ &= \sum_{\beta} (U^T)_{\alpha'\beta} e^{i\delta_{\beta}^J} \frac{\sin(pr - L' \pi/2 + \delta_{\beta}^J)}{pr} U_{\beta\alpha}. \end{aligned} \quad (4.21)$$

The expression above is real apart from the  $\exp(i\delta_{\beta}^J)$ . To eliminate this factor, the following linear combinations of the  $w(r)$ 's are introduced:

$$\begin{aligned} \frac{u_{\alpha',\alpha}^J}{r} &\equiv e^{-i\delta_{\alpha}^J} \sum_{\beta} \frac{w_{\alpha',\beta}^J}{r} (U^T)_{\beta\alpha} \\ &\simeq (U^T)_{\alpha'\alpha} [\cos \delta_{\alpha}^J j_{L'}(pr) - \sin \delta_{\alpha}^J n_{L'}(pr)], \end{aligned} \quad (4.22)$$

and the  $u(r)$ 's are then the sought real solutions of Eq. (4.15).

The asymptotic behavior of the  $u(r)$ 's can now be read off from Eq. (4.22) once the  $U$  matrices above have been constructed. The latter can be written, up to linear terms in the "small" mixing angles induced by  $v^{\text{PV}}$ , as

$$U = \begin{bmatrix} 1 & \epsilon_{12}^0 \\ -\epsilon_{12}^0 & 1 \end{bmatrix}, \quad J=0,$$

$$U = \begin{bmatrix} \cos \epsilon'_{12} & \sin \epsilon'_{12} & \epsilon'_{13} \cos \epsilon'_{12} + \epsilon'_{23} \sin \epsilon'_{12} & \epsilon'_{14} \cos \epsilon'_{12} + \epsilon'_{24} \sin \epsilon'_{12} \\ -\sin \epsilon'_{12} & \cos \epsilon'_{12} & -\epsilon'_{13} \sin \epsilon'_{12} + \epsilon'_{23} \cos \epsilon'_{12} & -\epsilon'_{14} \sin \epsilon'_{12} + \epsilon'_{24} \cos \epsilon'_{12} \\ -\epsilon'_{13} & -\epsilon'_{23} & 1 & 0 \\ -\epsilon'_{14} & -\epsilon'_{24} & 0 & 1 \end{bmatrix}, \quad J \geq 1.$$

Inverting the first line of Eq. (4.22),

$$\frac{w_{\alpha',\alpha}^J}{r} = \sum_{\beta} e^{i\delta_{\beta}^J} \frac{u_{\alpha',\beta}^J}{r} U_{\beta\alpha}, \quad (4.23)$$

and inserting the resulting expressions into Eq. (4.15) leads to the Schrödinger equations satisfied by the (real) functions  $u(r)$ . They are identical to those of Eq. (4.15), but for the  $w(r)$ 's being replaced by the  $u(r)$ 's. These equations are then solved by standard numerical techniques. Note that (i)  $v_{\alpha,\alpha}^J = v_{\alpha,\alpha}^{J,\text{PC}}$ , since the diagonal matrix elements of  $v^{\text{PV}}$  vanish because of parity selection rules; (ii) terms of the type  $r v_{\alpha',\beta}^{J,\text{PV}}(r) u_{\beta,\alpha}^J(r)/r$  involving the product of a PV potential matrix element with a  $v^{\text{PV}}$ -induced wave function are neglected.

Finally, the physical amplitude for  $np$  elastic scattering from an initial state with spin projections  $m_n, m_p$  to a final state with spin projections  $m'_n, m'_p$  is given by

$$\begin{aligned} \langle m'_n m'_p | M | m_n m_p \rangle &= \frac{1}{2} \sum_{S' M'_S T', SM_S T} (-)^{T+T'} \langle \frac{1}{2} m'_n, \frac{1}{2} m'_p | S' M'_S \rangle \\ &\times \langle \frac{1}{2} m_n, \frac{1}{2} m_p | SM_S \rangle M_{S' M'_S T', SM_S T}(E, \theta), \end{aligned} \quad (4.24)$$

where the amplitude  $M$  is related to the  $T$  matrix defined in Eq. (4.6) via

$$M_{S' M'_S T', SM_S T}(E, \theta) = -\frac{\mu}{2\pi} T(\mathbf{p}', S' M'_S T'; p \hat{z}, SM_S T), \quad (4.25)$$

and the factor  $(-1)^{T+T'}/2$  comes from the Clebsch-Gordan coefficients combining the neutron and proton states to total initial (final) isospin  $T(T')$ . Note that the direction of the initial momentum  $\mathbf{p}$  has been taken to define the spin quantization axis (the  $z$  axis),  $\theta$  is the angle between  $\hat{\mathbf{p}}$  and  $\hat{\mathbf{p}}'$ , the direction of the final momentum, and the energy  $E = p^2/(2\mu) [= p'^2/(2\mu)]$ . Using the expansion of the  $T$  matrix, Eq. (4.8) with  $v_{L' S' T', LST}^J$  replaced by  $T_{L' S' T', LST}^J$ , and the relation between the  $S$  and  $T$  matrices, Eq. (4.13), the amplitude induced by  $v^{\text{PC}} + v^{\text{PV}}$  can be expressed as

$$\begin{aligned} M_{S' M'_S T', SM_S T}(E, \theta) &= \sqrt{4\pi} \sum_{JLL'} \sqrt{2L+1} \epsilon_{\alpha'} \\ &\times \epsilon_{\alpha} \langle L' (M_S - M'_S), S' M'_S | JM_S \rangle \\ &\times \langle L0, SM_S | JM_S \rangle Y_{L'(M_S - M'_S)}(\theta) \\ &\times \frac{S'_{\alpha,\alpha}(p) - \delta_{\alpha',\alpha}}{ip}, \end{aligned} \quad (4.26)$$

where again  $\alpha(\alpha') = LST(L'S'T')$ .

### C. Momentum-space formulation

In order to consider the PC momentum space Bonn [11] and Nijmegen [10] potentials, it is useful to formulate the  $np$

scattering problem in  $p$  space. One way to accomplish this is to solve for the  $K$  matrix [34]

$$K_{\alpha',\alpha}^J(p';p) = v_{\alpha',\alpha}^J(p';p) + \frac{4\mu}{\pi} \int_0^\infty dk k^2 \sum_\beta v_{\alpha',\beta}^J(p';k) \times \frac{\mathcal{P}}{p^2 - k^2} K_{\beta,\alpha}^J(k;p), \quad (4.27)$$

where  $\mathcal{P}$  denotes a principal-value integration, and the  $p$ -space matrix elements of the potential are defined in Eq. (4.9). The integral equations (4.27) are discretized, and the resulting systems of linear equations are solved by direct numerical inversion. The principal-value integration is eliminated by a standard subtraction technique [35]. Once the  $K$  matrices in the various channels have been determined, the corresponding (on-shell)  $S$  matrices are obtained from

$$S^J(p) = [1 + 2i \mu p K^J(p;p)]^{-1} [1 - 2i \mu p K^J(p;p)], \quad (4.28)$$

and from these the amplitudes  $M_{S'M'_S T', SM_S T}(E, \theta)$ , Eq. (4.26), are constructed.

Some of the studies of PV effects in the  $np$  system of interest here, specifically those relative to the  $\bar{n}p$  radiative capture,  $d(\bar{\gamma}, n)p$  photodisintegration at threshold, and  $d(\bar{e}, e')np$  electrodisintegration in quasielastic kinematics, are more conveniently carried out in  $r$  space, and therefore require  $r$ -space wave functions. To this end, one first rewrites Eq. (4.11) in a compact notation as

$$\frac{w^J(r;p)}{r} = j(pr) - 2i \mu p j(pr) T^J(p;p) + \frac{4\mu}{\pi} \int_0^\infty dk k^2 j(kr) \frac{\mathcal{P}}{p^2 - k^2} T^J(k;p), \quad (4.29)$$

where the matrices  $[w^J(r;p)]_{\alpha',\alpha} \equiv w_{\alpha',\alpha}^J(r;p)$  and  $[j(pr)]_{\alpha',\alpha} \equiv \delta_{\alpha',\alpha} j_{L'}(pr)$  have been introduced for ease of presentation. Then, by making use of the following relation between the off-shell  $T$  and  $K$  matrices:

$$T^J(p';p) = K^J(p';p) - 2i \mu p K^J(p';p) T^J(p;p), \quad (4.30)$$

which on shell leads to

$$T^J(p;p) = [1 + 2i \mu p K^J(p;p)]^{-1} K^J(p;p), \quad (4.31)$$

one can simply express the  $w^J(r;p)$  matrix of solutions in terms of the previously determined  $K$  matrix as

$$\frac{w^J(r;p)}{r} = \left( j(pr) + \frac{4\mu}{\pi} \int_0^\infty dk k^2 j(kr) \frac{\mathcal{P}}{p^2 - k^2} K^J(k;p) \right) \times [1 + 2i \mu p K^J(p;p)]^{-1}. \quad (4.32)$$

The Bessel transforms above are carried out numerically by Gaussian integration over a uniform  $p$  grid extending up to momenta  $\approx 125 \text{ fm}^{-1}$ . The computer programs have been successfully tested by comparing, for the PC Argonne  $v_{18}$  [9]

and PV DDH [8] potentials,  $r$  space wave functions as obtained from Eq. (4.32) and by direct solution of the Schrödinger equations, Eq. (4.15).

#### D. The deuteron wave function

The deuteron state has  $J=1$  and its normalized wave function is written in  $r$  space as

$$\psi_{d,m_d}(\mathbf{r}) = \sum_{LST} i^L \epsilon_{LST} u_{LST}(r) \mathcal{Y}_{LS,J=1}^{m_d}(\hat{\mathbf{r}}) \eta_0^T. \quad (4.33)$$

It has PC components with  $LST=010$  and  $210$ , the standard  ${}^3S_1$  and  ${}^3D_1$  waves (however, note again the unconventional phase factor  $i^L$ , which makes the sign of the  $D$  wave opposite to that of the  $S$  wave), and PV components with  $LST=100$  and  $111$ , the  ${}^1P_1$  and  ${}^3P_1$  waves (which are real functions because of the phase choice above). The radial functions are determined by solving the Schrödinger equation (4.15) in the  $J=1$  channel with the boundary conditions  $u_{LST}(r) \propto r^L$  in the limit  $r \rightarrow 0$  and

$$u_{010}(r) \propto \frac{e^{-\kappa r}}{r}, \quad (4.34)$$

$$u_{210}(r) \propto \frac{e^{-\kappa r}}{r} \left( 1 + \frac{3}{\kappa r} + \frac{3}{(\kappa r)^2} \right), \quad (4.35)$$

$$u_{100}(r) \propto \frac{e^{-\kappa r}}{r} \left( 1 + \frac{1}{\kappa r} \right) \quad (4.36)$$

in the asymptotic region. The asymptotic behavior of  $u_{111}(r)$  is identical to that of  $u_{100}(r)$  above, and the constant  $\kappa$  denotes the combination  $\sqrt{2\mu|E_d|}$ , where  $|E_d|$  is the deuteron binding energy (2.225 MeV).

In  $p$  space the deuteron wave function is obtained from solutions of the homogeneous integral equations

$$\bar{u}_{LST}(p) = \frac{1}{E_d - p^2/(2\mu)} \frac{2}{\pi} \int_0^\infty dk k^2 \sum_{L'S'T'} v_{LST,L'S'T'}^{J=1}(p;k) \times \bar{u}_{L'S'T'}(k), \quad (4.37)$$

and from these

$$u_{LST}(r) = \frac{2}{\pi} \int_0^\infty dp p^2 j_L(pr) \bar{u}_{LST}(p). \quad (4.38)$$

Figure 2 displays the functions  $u_{LST}(r)$  obtained with the PC AV18 [9] (BONN [11]) and PV DDH-adj [8] potentials (the values for the coupling constants and cutoff parameters in the DDH potential are those listed in Table I). The PC  ${}^3S_1$  and  ${}^3D_1$  components are not very sensitive to the input PC potential. For example, most of the difference between the AV18 and BONN  ${}^3D_1$  waves is due to nonlocalities present in the one-pion-exchange (OPE) part of the BONN potential. In fact, it has been known for over two decades [36], and recently reemphasized by Amghar and Desplanques [37] and Forest [38], that the local and nonlocal OPE interactions are related to each other by a unitary transformation. Therefore



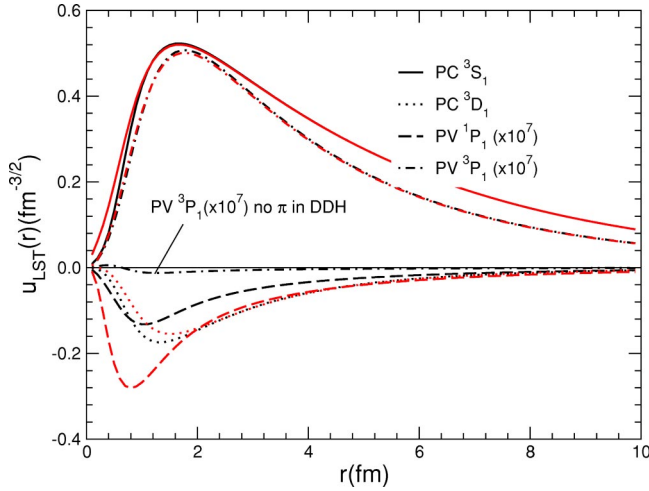


FIG. 2. (Color online) The deuteron PC  ${}^3S_1$  and  ${}^3D_1$  and PV  ${}^1P_1$  and  ${}^3P_1$  radial wave functions obtained with the (PC) AV18 or BONN and (PV) DDH-adj potentials. Also shown is the  ${}^3P_1$  wave function obtained with the AV18 and a truncated DDH potential (labeled “no  $\pi$  in DDH”), including only  $\rho$ - and  $\omega$ -meson exchange contributions. For the phase convention, see text.

the differences between local and nonlocal OPE cannot be of any consequence for the prediction of observables, such as binding energies and electromagnetic form factors, provided, of course, that three-body interactions and/or two-body currents generated by the unitary transformation are also included—see Ref. [39] for a recent demonstration of this fact within the context of a calculation of the deuteron structure function  $A(q)$  and tensor observable  $T_{20}(q)$  based on the local AV18 and nonlocal BONN potentials and associated (unitarily consistent) electromagnetic currents. This point was also stressed in Ref. [6].

The PV  ${}^3P_1$  component is, in magnitude, much larger than the  ${}^1P_1$ . This is easily understood, since the long-range  $\pi$ -exchange term in the DDH potential is nonvanishing only for transitions in which  $|T-T'|=1$ , and therefore does not contribute in the  ${}^1P_1$  channel. In this channel, however, the DDH  $\rho$ - and  $\omega$ -exchange terms play a role. Note that, because of the short-range character of the associated dynamics, the AV18 and BONN  ${}^1P_1$  waves show considerably more model-dependence than the corresponding  ${}^3P_1$  waves.

Finally, in Fig. 2 the PV  ${}^3P_1$  wave obtained with the AV18 and a truncated DDH potential, retaining only the short-range  $\rho$  and  $\omega$  exchanges, is also shown. The comparison between the  ${}^3P_1$  waves corresponding to the full and truncated DDH potentials demonstrates that this channel is indeed dominated by the  $\pi$ -exchange term in the DDH.

## V. PARITY-VIOLATING OBSERVABLES

In this section we give explicit expressions for parity-violating observables in the  $np$  system, including the longitudinal asymmetry and spin rotation in  $\vec{n}p$  elastic scattering, the photon asymmetry in  $\vec{n}p$  radiative capture, and the asymmetries in deuteron photodisintegration  $d(\vec{\gamma}, n)p$  in the threshold region and electrodisintegration  $d(\vec{e}, e')np$  in quasielastic kinematics.

### A. Longitudinal asymmetry and spin rotation in $\vec{n}p$ elastic scattering

The differential cross section for scattering of a neutron with initial polarization  $m_n$  is given by

$$\sigma_{m_n}(E, \theta) = \frac{1}{2} \sum_{m_p} \sum_{m'_n m'_p} |\langle m'_n m'_p | M | m_n m_p \rangle|^2, \quad (5.1)$$

and the longitudinal asymmetry is defined as

$$A(E, \theta) = \frac{\sigma_+(E, \theta) - \sigma_-(E, \theta)}{\sigma_+(E, \theta) + \sigma_-(E, \theta)}, \quad (5.2)$$

where  $\pm$  denote the initial polarizations  $\pm 1/2$ . The total asymmetry  $A(E)$ , integrated over the solid angle, then reads

$$A(E) = \frac{\int d\Omega \sigma(E, \theta) A(E, \theta)}{\int d\Omega \sigma(E, \theta)}, \quad (5.3)$$

where  $\sigma = (\sigma_+ + \sigma_-)/2$  is the spin-averaged differential cross section. The optical theorem allows  $A(E)$  to be simply expressed as

$$\begin{aligned} A(E) = & \text{Im} \sum_{T T'} \left( [(-)^{T+T'} - 1] M_{11T', 11T}(E, 0) + \frac{(-)^{T+T'}}{2} \right. \\ & \times \sum_{S S'} [1 - (-)^{S+S'}] M_{S'0T', S0T}(E, 0) \left. \right) \\ & \times \frac{1}{\text{Im} \sum_{SM_S T} M_{SM_S T, SM_S T}(E, 0)}, \end{aligned} \quad (5.4)$$

where in the equation above use has been made of the symmetry property

$$\begin{aligned} & M_{S', M'_S, T'; S, M_S, T}(E, \theta) \\ & = (-)^{T+T'} (-)^{M_S - M'_S} M_{S', -M'_S, T'; S, -M_S, T}(E, \theta). \end{aligned} \quad (5.5)$$

It is clear that the numerator of  $A(E)$  would vanish in the absence of PV interactions, since  $v^{\text{PC}}$ , in contrast to  $v^{\text{PV}}$ , cannot change the total spin  $S$  or isospin  $T$  of the  $np$  pair. In particular, the long-range part of  $v^{\text{PV}}$  due to pion exchange can only contribute to the first term in the numerator of Eq. (5.4), since it is diagonal in  $S$ , but nonvanishing for transitions  $|T-T'|=1$ .

The transmission of a low-energy neutron beam through matter is described in terms of an index of refraction. A heuristic argument, outlined in Ref. [40], and the more rigorous—although less transparent—derivation presented in Ref. [34] show that a neutron with spin projection  $|m_n\rangle$ , after traversing a slab of width  $d$  of matter, is described by an asymptotic wave function given by

$$e^{ip(z-d)} e^{ip d n_{m_n}} |m_n\rangle, \quad (5.6)$$

where  $\mathbf{p} = \mathbf{p}_n/2$  is the initial relative momentum (assumed along the  $z$  axis), and the index of refraction  $n_{m_n}$  is related to

the density  $\rho$  of scattering centers in matter and the forward scattering amplitude. For the specific case under consideration here—neutron scattering from hydrogen—this relation reads

$$n_{m_n} - 1 = \frac{2\pi\rho}{p^2} \frac{1}{2} \sum_{m_p} \langle m_n m_p | M | m_n m_p \rangle |_{\theta=0}. \quad (5.7)$$

Thus a neutron, initially polarized in the  $x$  direction,

$$e^{ipz}(|+\rangle + |-\rangle)/\sqrt{2}, \quad (5.8)$$

having traversed a slab of matter, is described in the asymptotic region by a wave function given by

$$e^{ip(z-d)} e^{ip d(n_+ + n_-)/2} (e^{ip d(n_+ - n_-)/2} |+\rangle + e^{-ip d(n_+ - n_-)/2} |-\rangle)/\sqrt{2}. \quad (5.9)$$

In the absence of  $v^{\text{PV}}$ , the difference  $n_+ - n_-$  vanishes, since it is proportional to the sum over  $T, T'$  in the numerator of Eq. (5.4), while

$$\frac{\text{Im}(n_+ + n_-)}{2} = \frac{\rho}{2p} \sigma, \quad (5.10)$$

where  $\sigma$  is the spin-averaged cross section introduced above, and hence there will be an attenuation in the beam flux proportional to  $\exp(-\rho d \sigma)$ . The real part of  $(n_+ + n_-)/2$  instead generates an unobservable phase factor.

However, if PV interactions are present, then the real part of the (now nonvanishing) difference  $n_+ - n_-$  leads to a rotation of the neutron polarization by an angle  $\phi$  explicitly given by [41–43]

$$\begin{aligned} \phi = & -\frac{2\pi\rho d}{p} \frac{1}{2} \sum_{m_p} \text{Re}[\langle +, m_p | M | +, m_p \rangle \\ & - \langle -, m_p | M | -, m_p \rangle]_{\theta=0}. \end{aligned} \quad (5.11)$$

### B. Photon asymmetry in $\vec{n}\vec{p}$ radiative capture

In the center-of-mass (c.m.) frame, the radiative transition amplitude between an initial continuum state with neutron and proton in spin-projection states  $m_n$  and  $m_p$ , respectively, and in relative momentum  $\mathbf{p}$ , and a final deuteron state in spin-projection state  $m_d$ , recoiling with momentum  $-\mathbf{q}$ , is given by

$$j_{\lambda m_d, m_n m_p}^{(+)}(\mathbf{p}\hat{\mathbf{z}}, \mathbf{q}) = \langle -\mathbf{q}; m_d | \hat{\epsilon}_\lambda^*(\mathbf{q}) \cdot \mathbf{j}^\dagger(\mathbf{q}) | \mathbf{p}\hat{\mathbf{z}}, m_n m_p \rangle^{(+)}, \quad (5.12)$$

where  $\mathbf{q}$  is the momentum of the emitted photon and  $\hat{\epsilon}_\lambda(\mathbf{q})$ ,  $\lambda = \pm 1$ , are the spherical components of its polarization vector, and  $\mathbf{j}(\mathbf{q})$  is the nuclear electromagnetic current operator. Note that  $\hat{\mathbf{p}}$  has been taken along the  $z$  axis, the spin-quantization axis.

The initial  $np$  continuum state, satisfying outgoing-wave boundary conditions, is related to that constructed in Sec. IV A via

$$\begin{aligned} |p\hat{\mathbf{z}}, m_n m_p \rangle^{(+)} &= \frac{1}{\sqrt{2}} \sum_{ST} (-)^{T+1} \langle \frac{1}{2} m_n, \frac{1}{2} m_p | SM_S \rangle |p\hat{\mathbf{z}}, SM_S, T \rangle^{(+)} \\ &= \sqrt{4\pi} \sum_{J\alpha} \bar{\epsilon}_\alpha \sqrt{2L+1} \langle \frac{1}{2} m_n, \frac{1}{2} m_p | SM_S \rangle \\ &\quad \times \langle L0, SM_S | JM_S \rangle |JM_S, \alpha \rangle^{(+)}, \end{aligned} \quad (5.13)$$

where in the first equality the factor  $(-)^{T+1}/\sqrt{2}$  is from a Clebsch-Gordan coefficient combining the neutron and proton states to total isospin  $T$ , and in the second equality  $\bar{\epsilon}_\alpha \equiv (-)^T \epsilon_\alpha$  and the states  $|JM_S, \alpha \rangle^{(+)}$  have wave functions

$$\langle \mathbf{r} | JM_S, \alpha \rangle^{(+)} = \sum_{\alpha'} i^{L'} \epsilon_{\alpha'} \frac{w_{\alpha', \alpha}^J(r; p)}{r} \mathcal{Y}_{L'S', J}^{MJ}(\hat{\mathbf{r}}) \eta_0^{T'}, \quad (5.14)$$

with  $\alpha = LST$  and similarly for  $\alpha'$ . The quantum numbers  $\alpha$  and  $\alpha'$  characterize the incoming and outgoing waves, respectively.

The c.m. differential cross section for capture of a neutron with spin projection  $m_n$  is then written as

$$\sigma_{m_n}^\gamma(\theta) = \frac{\sigma_0}{2} \sum_{m_p, \lambda, m_d} |j_{\lambda m_d, m_n m_p}^{(+)}(\mathbf{p}\hat{\mathbf{z}}, \mathbf{q})|^2, \quad (5.15)$$

where  $\theta$  is the angle between  $\hat{\mathbf{z}}$  and  $\hat{\mathbf{q}}$  and

$$\sigma_0 = \frac{\alpha}{2\pi v} \frac{q}{1 + q/m_d}. \quad (5.16)$$

Here  $\alpha$  is the fine-structure constant,  $m_d$  is the deuteron mass,  $v$  is the relative velocity,  $v = p/\mu$ , and the photon energy  $q$  is given by

$$q = m_d \left[ -1 + \sqrt{1 + \frac{2}{m_d} \left( |E_d| + \frac{p^2}{2\mu} \right)} \right] \simeq |E_d| + \frac{p^2}{2\mu}. \quad (5.17)$$

The photon asymmetry  $A^\gamma(\theta)$  is defined as in Eq. (5.2) with  $\sigma_{m_n}(\theta)$  replaced by  $\sigma_{m_n}^\gamma(\theta)$ . By expanding the matrix elements of the current operator in terms of reduced matrix elements (RMEs) of electric ( $E_l$ ) and magnetic ( $M_l$ ) multipole operators as [29]

$$\begin{aligned} \langle -\mathbf{q}; m_d | \hat{\epsilon}_\lambda^*(\mathbf{q}) \cdot \mathbf{j}^\dagger(\mathbf{q}) | JM_S, \alpha \rangle^{(+)} \\ = -\sqrt{2\pi} \sum_{l_z} (-i)^l \sqrt{\frac{2l+1}{3}} \langle JM_S, l l_z | 1 m_d \rangle d_{l_z, -\lambda}^l(-\theta) \\ \times [E_l(J, \alpha) + \lambda M_l(J, \alpha)], \end{aligned} \quad (5.18)$$

with

$$X_l(J, \alpha) \equiv \langle d, J = 1 || X_l || J, \alpha \rangle^{(+)} \quad (5.19)$$

and  $X_l = E_l$  or  $M_l$ , one finds, by retaining the  $^1S_0$  and  $^3S_1$  channels in the sum over  $\alpha$  in Eq. (5.13), the only relevant incoming waves in the energy regime of interest here (fractions of eV),

$$A^\gamma(\theta) = a^\gamma \cos \theta, \quad (5.20)$$

where  $a^\gamma$  is given by

$$a^\gamma = \frac{-\sqrt{2} \operatorname{Re} [M_1^*(^1S_0)E_1(^3S_1) + E_1^*(^1S_0)M_1(^3S_1)] + \operatorname{Re} [E_1^*(^3S_1)M_1(^3S_1)]}{|M_1(^1S_0)|^2 + |E_1(^1S_0)|^2 + |M_1(^3S_1)|^2 + |E_1(^3S_1)|^2}, \quad (5.21)$$

and in Eq. (5.18) the  $d_{l_z, l'_z}^j$  are standard rotation matrices [44]. The  $E_l(J, \alpha)$  and  $M_l(J, \alpha)$  RMEs should carry a superscript (+); it has been dropped for ease of presentation.

Several comments are now in order. First, the photon asymmetry has the expected dependence on  $\cos \theta$ , since  $A^\gamma(\theta) \propto \sigma_n \cdot \hat{\mathbf{q}}$ . Note that the contributions of higher-order multipole operators with  $l=2$  have been ignored in the equation above.

Second, because of the definition of the states in Eq. (5.14), a generic RME  $X_l(J\alpha)$  is expressed as

$$X_l(J\alpha) = \sum_{\alpha'} X_l(J\alpha', \alpha), \quad (5.22)$$

namely, as a sum over the contributions of outgoing channels  $\alpha'$  corresponding to an incoming channel  $\alpha$ ; for example,

$$M_1(^1S_0) = M_1(^1S_0, ^1S_0) + M_1(^3P_0, ^1S_0). \quad (5.23)$$

Third, in the absence of parity-violating interactions, the only surviving RMEs are the  $M_1(^1S_0, ^1S_0)$ ,  $M_1(^3S_1, ^3S_1)$ , and  $M_1(^3D_1, ^3S_1)$ , and therefore the parameter  $a^\gamma$  vanishes. Furthermore, the  $M_1(^3S_1, ^3S_1)$  RME also vanishes due to orthogonality of the initial and final states (in the limit in which isoscalar two-body currents are neglected), while the

$M_1(^3D_1, ^3S_1)$  RME is suppressed in the energy regime of interest here. Thus, the standard result for the spin-averaged radiative capture cross section, integrated over the solid angle, follows:

$$\sigma^\gamma = (4\pi)^2 \sigma_0 |M_1(^1S_0, ^1S_0)|^2. \quad (5.24)$$

Lastly, when PV interactions are present, the analysis is more delicate, since then, in addition to admixing small opposite-parity components into the wave functions corresponding to  $v^{\text{PC}}$ , these interactions also induce two-body terms in the electromagnetic current operator, as discussed in Sec. III. Thus,  $\mathbf{j} = \mathbf{j}^{\text{PC}} + \mathbf{j}^{\text{PV}}$ , where  $\mathbf{j}^{\text{PC}}$  includes the convection and spin-magnetization currents of single nucleons as well as the two-body currents associated with  $v^{\text{PC}}$ , while  $\mathbf{j}^{\text{PV}}$  includes those terms generated by  $v^{\text{PV}}$ . The multipole operators can then be written as  $X_{ll_z} = X_{ll_z}^{\text{PC}} + X_{ll_z}^{\text{PV}}$ , and those constructed from  $\mathbf{j}^{\text{PV}}$  have unnatural parities, namely,  $(-)^l$  for  $M_{ll_z}^{\text{PV}}$  and  $(-)^{l+1}$  for  $E_{ll_z}^{\text{PV}}$ . Therefore, for example, the RMEs  $M_1(^1S_0, ^1S_0)$  and  $M_1^{\text{PV}}(^1S_0, ^1S_0)$  connect the PC  $^1S_0$  state to, respectively, the PC and PV components of the deuteron. A straightforward analysis then shows that, up to linear terms in effects induced by  $v^{\text{PV}}$  in either the wave functions or currents, the parameter  $a^\gamma$  is given by

$$a^\gamma = \frac{-\sqrt{2} \operatorname{Re} \{M_1^*(^1S_0, ^1S_0)[E_1(^3S_1, ^3S_1) + E_1(^3D_1, ^3S_1) + E_1(^3P_1, ^3S_1)]\}}{|M_1(^1S_0, ^1S_0)|^2}, \quad (5.25)$$

where again terms containing the RMEs  $M_1(^3S_1, ^3S_1)$  and  $M_1(^3D_1, ^3S_1)$  have been neglected. In the expression above, the RME  $E_1(^1P_1, ^3S_1)$  has also been neglected, since transitions induced by the isoscalar electric dipole operator are strongly suppressed [45,46]. Thus, the only relevant transitions are those connecting the  $^3P_1$  PV  $np$  state to the PC deuteron component and the  $^3S_1$  and  $^3D_1$  PC  $np$  states to the  $^3P_1$  PV deuteron component.

### C. Helicity-dependent asymmetry in $d(\vec{\gamma}, n)p$ photodisintegration

The relevant matrix element in the photodisintegration of a deuteron initially at rest in the laboratory is

$$j_{m_n m_p, \lambda m_d}^{(-)}(\mathbf{p}, \mathbf{q}) = \langle \mathbf{q}; \mathbf{p}, m_n m_p | \hat{\epsilon}_\lambda(\mathbf{q}) \cdot \mathbf{j}(\mathbf{q}) | m_d \rangle \quad (5.26)$$

in the notation of Sec. V B above. Here  $|\mathbf{q}; \mathbf{p}, m_n m_p\rangle^{(-)}$  represents an  $np$  scattering state with total momentum  $\mathbf{q}$  and

relative momentum  $\mathbf{p}$ , satisfying incoming-wave boundary conditions. Its (internal) wave function has the same partial-wave expansion given in Eq. (4.10), except for the replacement  $w_{\alpha', \alpha}^f(r) \rightarrow [w_{\alpha', \alpha}^f(r)]^*$ .

The cross section for absorption of a photon of helicity  $\lambda$ , summed over the final states and averaged over the initial spin projections of the deuteron, reads

$$\begin{aligned} \sigma_\lambda^\gamma &= \sum_i \sum_f 2\pi \delta(q + E_d - E_f) \frac{2\pi \alpha}{q} |j_{m_n m_p, \lambda m_d}^{(-)}(\mathbf{p}, \mathbf{q})|^2 \\ &= \frac{8\pi^2 \alpha}{3} \mu p \sum_{J\alpha} \sum_{l \geq 1} \epsilon_\alpha |\lambda M_l^{(-)}(J, \alpha) + E_l^{(-)}(J, \alpha)|^2, \end{aligned} \quad (5.27)$$

where  $E_f$  is the energy of the final state,

$$E_f = \frac{q^2}{2(m_n + m_p)} + \frac{p^2}{2\mu}, \quad (5.28)$$

and

$$\bar{\sum}_{i f} \equiv \frac{1}{3} \sum_{m_d} \sum_{m_n m_p} \int \frac{d\mathbf{p}}{(2\pi)^3} \frac{1}{2}. \quad (5.29)$$

Note that the factor 1/2 above is introduced to avoid double-counting the final states, and that the dependence upon the boundary condition of the continuum wave functions, the superscript  $(-)$ , has been reinserted in the RMEs of the electric and magnetic multipoles, namely,

$$X_l^{(-)}(J, \alpha) \equiv \langle J, \alpha | X_l | d, J=1 \rangle \quad (5.30)$$

and  $X_l = E_l$  or  $M_l$ .

The resulting PV asymmetry, defined as  $P^\gamma = (\sigma_+^\gamma - \sigma_-^\gamma) / (\sigma_+^\gamma + \sigma_-^\gamma)$ , is expressed as [68]

$$P^\gamma = \frac{\sum_{J\alpha} \sum_{l \geq 1} \epsilon_\alpha [M_l^{(-)}(J, \alpha) E_l^{(-)*}(J, \alpha) + \text{c.c.}]}{\sum_{J\alpha} \sum_{l \geq 1} \epsilon_\alpha [|M_l^{(-)}(J, \alpha)|^2 + |E_l^{(-)}(J, \alpha)|^2]} \quad (5.31)$$

and therefore vanishes unless (i) the initial and/or final states do not have definite parity (as is the case here because of the presence of PV  $NN$  interactions) and/or (ii) the electric and magnetic multipole operators have unnatural parities  $(-)^{l+1}$  and  $(-)^l$ , respectively, because of two-body PV electromagnetic currents associated with PV  $NN$  interactions [7].

It is easily shown that in the inverse process  $p(n, \vec{\gamma})d$  the expression for the photon circular polarization parameter is identical to that given above, but for the RMEs  $E_l^{(-)}$  and  $M_l^{(-)}$  being replaced by the corresponding  $E_l^{(+)}$  and  $M_l^{(+)}$ , defined in the previous section. Indeed, by making use of the transformation properties of the states and electric and magnetic multipole operators under time reversal  $\mathcal{T}$ ,

$$\mathcal{T} |d, m_d\rangle = (-)^{m_d-1} |d, -m_d\rangle, \quad (5.32)$$

$$\mathcal{T} |J, M_J; \alpha\rangle^{(+)} = (-)^{M_J-J} |J, -M_J; \alpha\rangle^{(-)}, \quad (5.33)$$

$$\mathcal{T} X_{l, l_z} \mathcal{T}^\dagger = (-)^{l_z} X_{l, -l_z}, \quad (5.34)$$

one finds the following relation for the RMEs:

$$E_l^{(+)}(J, \alpha) = (-)^{J+l} E_l^{(-)}(J, \alpha), \quad (5.35)$$

and similarly for the  $M_l$ 's. Hence, the circular polarizations measured in the direct and inverse processes are the same.

#### D. Longitudinal asymmetry in $d(\vec{e}, e')np$ electrodisintegration

The longitudinal asymmetry in the inclusive scattering of polarized electrons off a nuclear target results from the interference of amplitudes associated with photon and  $Z^0$  exchanges as well as from the presence of parity-violating components in the nucleon-nucleon interaction. For completeness, we summarize below the relevant formulas. The

initial and final electron (nucleus) four-momenta are labeled by  $k^\mu$  and  $k'^\mu$  ( $P^\mu$  and  $P'^\mu$ ), respectively, while the four-momentum transfer  $q^\mu$  is defined as  $q^\mu \equiv k^\mu - k'^\mu \equiv (\omega, \mathbf{q})$ . The amplitudes for the  $\gamma$ - and  $Z$ -exchange processes are then given by [47]

$$M = -\frac{4\pi\alpha}{q_\mu^2} (M^\gamma + M^Z), \quad (5.36)$$

$$M^\gamma = \bar{u}' \gamma^\sigma u j_{\sigma, fi}^\gamma, \quad (5.37)$$

$$M^Z = \frac{1}{4\pi\sqrt{2}} \frac{G_\mu q_\mu^2}{\alpha} \bar{u}' \gamma^\sigma (g_V^{(e)} + g_A^{(e)} \gamma_5) u j_{\sigma, fi}^Z, \quad (5.38)$$

where  $G_\mu$  is the Fermi constant for muon decay,  $g_V^{(e)} = -1 + 4 \sin^2 \theta_W$  and  $g_A^{(e)} = 1$  are the standard model values for the neutral-current couplings to the electron given in terms of the Weinberg angle  $\theta_W$ ,  $u$  and  $u'$  are the initial and final electron spinors, and  $j_{fi}^{\gamma, \sigma}$  and  $j_{fi}^{Z, \sigma}$  denote matrix elements of the electromagnetic and weak neutral currents, i.e.,

$$j_{fi}^{\gamma, \sigma} \equiv \langle f | j^{\gamma, \sigma}(0) | i \rangle \equiv (\rho_{fi}^\gamma(\mathbf{q}), \mathbf{j}_{fi}^\gamma(\mathbf{q})), \quad (5.39)$$

and similarly for  $j_{fi}^{Z, \sigma}$ . Here  $|i\rangle$  and  $|f\rangle$  represent the initial deuteron state and final  $np$  scattering state with incoming-wave boundary conditions [the  $(-)$  solution], respectively. Note that in the amplitude  $M^Z$  the  $q_\mu^2$  dependence of the  $Z^0$  propagator has been ignored, since  $|q_\mu^2| \ll m_Z^2$ .

The parity-violating asymmetry  $A$  is given by the ratio of the difference over the sum of the inclusive cross sections  $d\sigma_h/d\Omega d\omega$  for incident electrons with helicities  $h = \pm 1$ . It depends on the three-momentum and energy transfers  $q$  and  $\omega$  and scattering angle  $\theta_e$  of the electron and is conveniently expressed as

$$A = A_{\gamma\gamma} + A_{\gamma Z}. \quad (5.40)$$

Standard manipulations then lead to the following expression for the asymmetry in the extreme relativistic limit for the electron [32,47]:

$$A_{\gamma\gamma} = \frac{v_T R_T^{\gamma, \gamma}}{v_L R_L^{\gamma, \gamma} + v_T R_T^{\gamma, \gamma}}, \quad (5.41)$$

$$A_{\gamma Z} = \frac{1}{2\sqrt{2}} \frac{G_\mu Q^2}{\pi \alpha} \frac{g_A^{(e)} v_L R_L^{\gamma, 0} + g_A^{(e)} v_T R_T^{\gamma, 0} + g_V^{(e)} v_T R_T^{\gamma, 5}}{v_L R_L^{\gamma, \gamma} + v_T R_T^{\gamma, \gamma}}, \quad (5.42)$$

where the  $v$ 's are defined in terms of electron kinematical variables,

$$v_L = \frac{q_\mu^4}{q^4}, \quad (5.43)$$

$$v_T = \tan^2(\theta_e/2) + \frac{|q_\mu^2|}{2q^2}, \quad (5.44)$$

$$v_{T'} = \tan(\theta_e/2) \sqrt{\tan^2(\theta_e/2) + \frac{|q_\mu^2|}{q^2}}. \quad (5.45)$$

The  $R$ 's are the nuclear electroweak response functions, which depend on  $q$  and  $\omega$ , to be defined below. To this end, it is first convenient to separate the weak current  $j^{Z,\sigma}$  into its vector  $j^{0,\sigma}$  and axial-vector  $j^{5,\sigma}$  components, and to write correspondingly

$$j_{fi}^{Z,\sigma} = j_{fi}^{0,\sigma} + j_{fi}^{5,\sigma} \equiv (\rho_{fi}^0(\mathbf{q}), \mathbf{j}_{fi}^0(\mathbf{q})) + (\rho_{fi}^5(\mathbf{q}), \mathbf{j}_{fi}^5(\mathbf{q})). \quad (5.46)$$

The response functions can then be expressed as

$$R_L^{\gamma,a}(q, \omega) = \overline{\sum}_{i f} \delta(\omega + E_d - E_f) \text{Re}[\rho_{fi}^\gamma(\mathbf{q}) \rho_{fi}^{a*}(\mathbf{q})], \quad (5.47)$$

$$R_T^{\gamma,a}(q, \omega) = \overline{\sum}_{i f} \delta(\omega + E_d - E_f) \text{Re}[\mathbf{j}_{T,fi}^\gamma(\mathbf{q}) \cdot \mathbf{j}_{T,fi}^{a*}(\mathbf{q})], \quad (5.48)$$

$$R_{T'}^{\gamma,b}(q, \omega) = \overline{\sum}_{i f} \delta(\omega + E_d - E_f) \text{Im}[\mathbf{j}_{fi}^\gamma(\mathbf{q}) \times \mathbf{j}_{fi}^{b*}(\mathbf{q})]_z, \quad (5.49)$$

where  $E_d$  is the ground-state energy of the deuteron (assumed at rest in the laboratory),  $E_f$  is the energy of the final scattering state, and in Eqs. (5.47) and (5.48) [Eq. (5.49)] the superscript a (b) is either  $\gamma$  or 0 ( $\gamma$  or 5). Note that there is a sum over the final states and an average over the initial spin projections of the deuteron. In the expressions above for the  $R$ 's, it has been assumed that the three-momentum transfer  $\mathbf{q}$  is along the  $z$  axis, which defines the spin quantization axis for the nuclear states.

The asymmetry induced by hadronic weak interactions,  $A_{\gamma\gamma}$ , is easily seen to be proportional to the interference of electric and magnetic multipole contributions as in Eq. (5.31); indeed

$$\frac{(2\pi)^2 \alpha}{q} R_{T'}^{\gamma,\gamma} = \sigma_+^\gamma - \sigma_-^\gamma, \quad (5.50)$$

namely,  $R_{T'}^{\gamma,\gamma}$  is related, of course for  $\omega=q$ , to the difference of helicity-dependent photodisintegration cross sections. Similar considerations to those in Sec. V C allow one to conclude that this response would vanish in the absence of PV  $NN$  interactions (note, however, that in the present case there is, in addition to two-body PV currents, also a one-body PV term originating from radiative electroweak corrections, the anapole current [24]).

## VI. CALCULATION

In this section we briefly review the techniques used to calculate the PV observables in the  $np$  system—these are similar to those discussed most recently in Ref. [32].

The deuteron wave function in Eq. (4.33) is written, for each spatial configuration  $\mathbf{r}$ , as a vector in the spin-isospin space of the two nucleons,

$$\psi_{d,m_d}(\mathbf{r}) = \sum_{n=1}^8 \psi_{d,m_d}^{(n)}(\mathbf{r}) |n\rangle, \quad (6.1)$$

where  $|n\rangle = (p\uparrow)_1(n\uparrow)_2, (n\uparrow)_1(p\uparrow)_2, \dots, (n\downarrow)_1(p\downarrow)_2$  and  $\psi_{d,m_d}^{(n)}$  are the components of  $\psi_{d,m_d}$  in this basis. The scattering wave function in Eq. (4.10) is first approximated by retaining PC and PV interaction effects in all channels up to a certain preselected  $J_{\max}$  and by using spherical Bessel function for channels with  $J > J_{\max}$ , and is then expanded, for any given  $\mathbf{r}$ , in the same basis  $\{|n\rangle\}$  defined above. The radial functions  $w_{\alpha',\alpha}$  are obtained with the methods discussed in Sec. IV C.

Matrix elements of the electromagnetic (and neutral weak) current operators are written schematically as

$$\langle \psi_f | O | \psi_i \rangle = \int d\mathbf{r} \sum_{m,n} \psi_f^{(m)*}(\mathbf{r}) O_{m,n}(\mathbf{r}) \psi_i^{(n)}(\mathbf{r}). \quad (6.2)$$

The spin-isospin algebra is performed exactly with techniques similar to those developed in Ref. [17], while the  $\mathbf{r}$  space integrations are carried out efficiently by Gaussian quadratures. Note that no multipole expansion of the transition operators is required.

Extensive and independent tests of the computer programs have been completed successfully.

## VII. RESULTS AND DISCUSSION

In this section we present results for the longitudinal asymmetry and spin rotation in  $\vec{n}p$  elastic scattering, the photon asymmetry in the  $\vec{n}p$  radiative capture at thermal energies, and the asymmetries in the threshold photodisintegration and quasielastic electrodisintegration of the deuteron. To provide an estimate for the model dependence of these results, we consider several different high-quality interactions fit to strong-interaction data, the Argonne  $v_{18}$  [9], Bonn [11], and Nijmegen-I [10] interactions. We adopt the standard DDH [8] one-boson-exchange model of the parity-violating interaction, and solve the Schrödinger equation for the scattering state and deuteron bound state with the methods discussed in Sec. IV. The values for the meson-nucleon coupling constants and cutoff parameters in the DDH-adj model are those listed in Table I. Note that we have rescaled the  $\rho$ - and  $\omega$ -meson weak couplings occurring in the  $T=1$  channel so as to reproduce the  $\vec{p}p$  longitudinal asymmetry [6]. Only one linear combination is significantly constrained by the fit to the  $\vec{p}p$  experiment in the DDH-adj. As in the earlier analysis of scattering, the cutoff values in the meson-exchange interaction are taken from the BONN potential.

It is also useful to introduce here some of the notation adopted in the following subsections to denote variations on the DDH model defined above. The PV interaction denoted as DDH corresponds to a DDH model with  $\pi$ ,  $\rho$ , and  $\omega$  weak-coupling constants as specified by the “best value” set of Ref. [8], while the PV interaction denoted as DDH $\pi$  includes only the  $\pi$ -exchange term in the DDH model with the “best value” for the weak  $\pi NN$  coupling constant; see Table II.

Finally, while the short-range contributions to the PV interaction should not be viewed as resulting solely from the

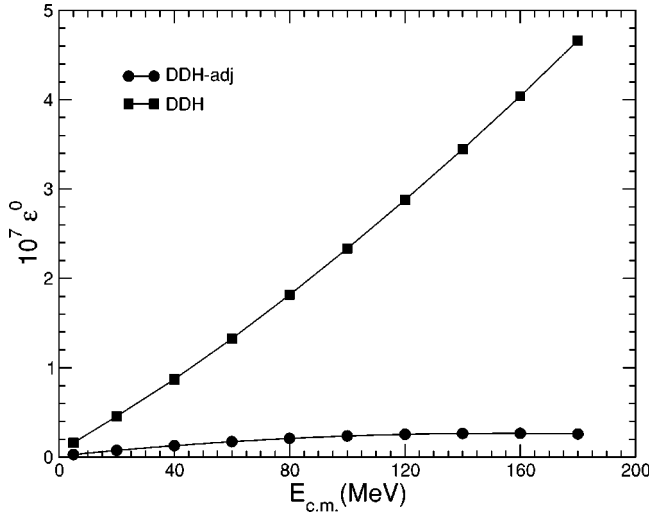


FIG. 3. The  $^1S_0$ - $^3P_0$  mixing parameter obtained with the AV18 model in combination with either of two variations of the DDH model, labeled DDH-adj and DDH (“best values”); see text.

exchange of single mesons, the six parameters of the DDH model are still useful in characterizing all the low-energy PV mixings. For example, two-pion exchange could play a role [48]; however, we assume that its effects can be included, at least at low energy, through the present combination of pion and short-range terms.

#### A. Longitudinal asymmetry and neutron spin rotation

In this section we present results for the longitudinal asymmetry and neutron spin rotation in  $\vec{n}p$  elastic scattering.

Figures 3–7 show the mixing parameters  $\epsilon_{lm}^J$  induced by the AV18 model in combination with the DDH-adj, DDH, and DDH  $\pi$  interactions. Only those  $\epsilon_{lm}^J$  induced by the PV interaction are displayed, namely, for  $J=0$   $\epsilon_{12}^0$  and for  $J \geq 1$

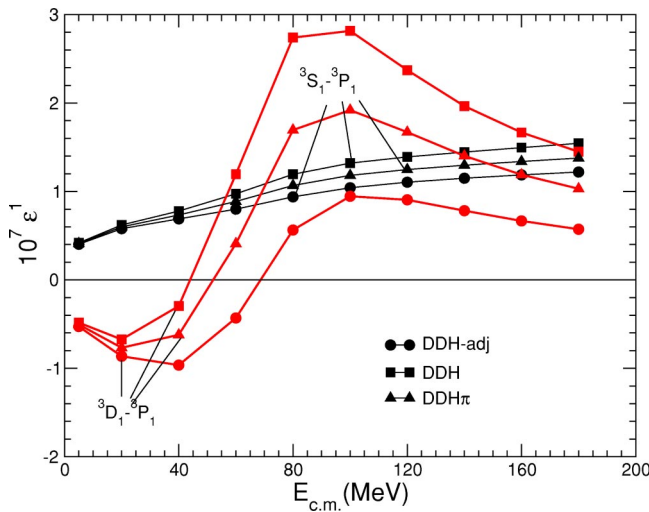


FIG. 4. (Color online) The  $^3S_1$ - $^3P_1$  and  $^3D_1$ - $^3P_1$  mixing parameters obtained with the AV18 model in combination with either of three variations of the DDH model, labeled DDH-adj, DDH, and DDH $\pi$ ; see text.

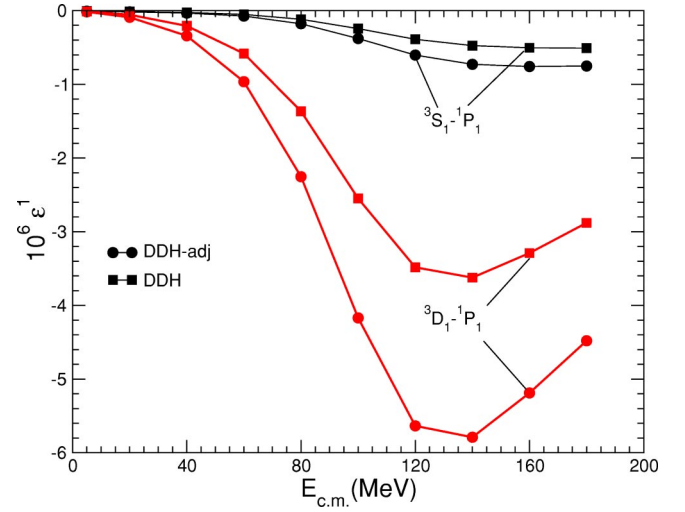


FIG. 5. (Color online) The  $^3S_1$ - $^1P_1$  and  $^3D_1$ - $^1P_1$  mixing parameters obtained with the AV18 model in combination with either of two variations of the DDH model, labeled DDH-adj and DDH; see text.

$\epsilon_{lm}^J$  with  $l=1, 2$  and  $m=3, 4$  in the notation of Tables III and IV.

The definitions adopted for the phase shifts and mixing parameters are those introduced in Sec. IV B. Up to linear terms in  $v^{PV}$ , the  $\delta_\alpha^J$  and  $\epsilon_{12}^{J \geq 1}$  values are not affected by weak interactions, and are determined solely by the strong interaction. They are identical to those listed in Ref. [9], but for two differences. First, the Blatt-Biedenharn parametrization is used here for the  $S$  matrix [49] rather than the bar-phase parametrization of it [50] employed in Ref. [9]. Second, because of the phase choice in the potential components [see Eq. (4.16) and comment below it], the mixing parameters  $\epsilon_{12}^{J \geq 1}$  have opposite signs relative to those listed in Ref. [9].

The coupling between channels with the same pair isospin  $T$  is induced by the short-range part of the DDH interaction, associated with vector-meson exchanges; its long-range component, due to pion exchange, vanishes in this case. As a

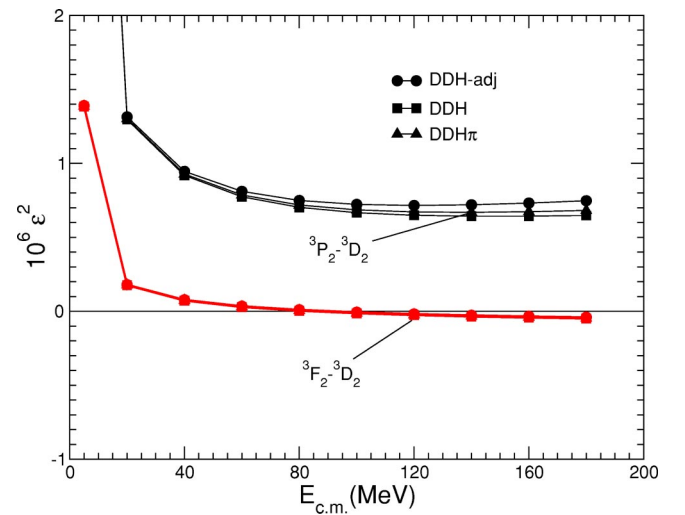


FIG. 6. (Color online) Same as in Fig. 4, but for the mixing parameters  $^3P_2$ - $^3D_2$  and  $^3F_2$ - $^3D_2$ .

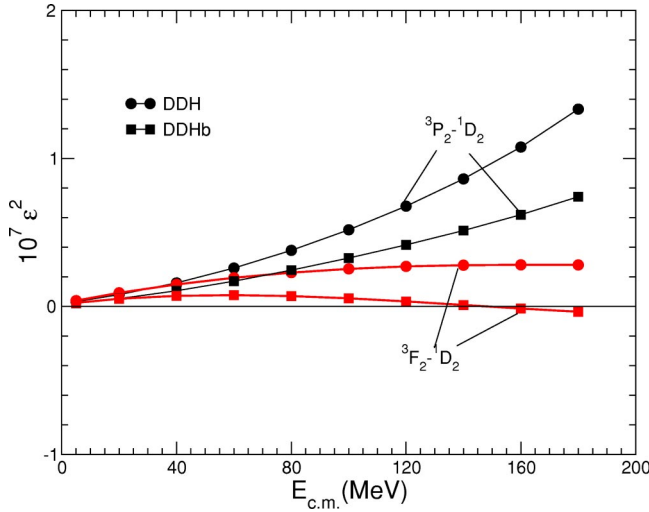


FIG. 7. (Color online) Same as in Fig. 5, but for the mixing parameters  ${}^3P_2\text{-}{}^1D_2$  and  ${}^3F_2\text{-}{}^1D_2$ .

result, the mixing parameters in Figs. 3, 5, and 7, calculated with the DDH-adj and DDH models, are rather different, reflecting the large differences in the values for some of the strong- and weak-coupling constants and short-range cut-offs between these two models; see Tables I and II.

The mixing parameters between channels with  $|\Delta T|=1$ , Figs. 4 and 6, in which the pion-exchange term is present, are still rather sensitive to the short-range behavior of the PV interaction, as reflected again by the differences in the DDH-adj and DDH predictions. However, this sensitivity is much reduced for the more peripheral waves, such as the  ${}^3P_2\text{-}{}^3D_2$  and  ${}^3F_2\text{-}{}^3D_2$  channels.

Figures 8–10 are meant to illustrate the sensitivity of the mixing angles to the input strong-interaction potential, which can be quite large, particularly in channels such as the  ${}^3D_1\text{-}{}^3P_1$  and  ${}^3D_1\text{-}{}^1P_1$ .

The total longitudinal asymmetry, defined in Eq. (5.3), is shown in Fig. 11 for a number of combinations of strong- and weak-interaction potentials. The asymmetries were cal-

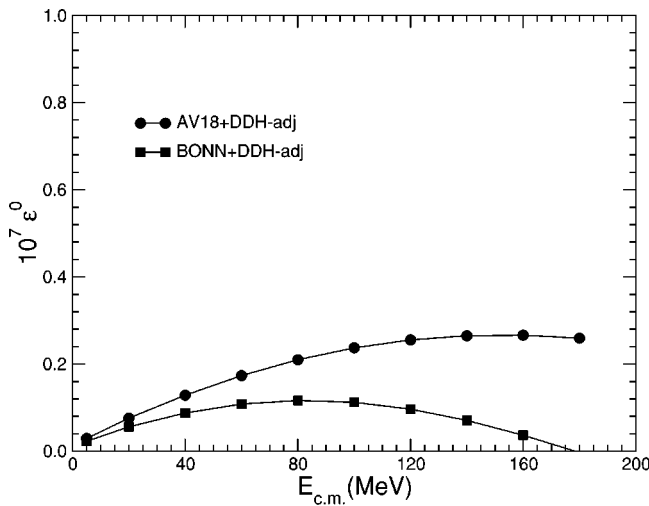


FIG. 8. The  ${}^1S_0\text{-}{}^3P_0$  mixing parameter obtained with the DDH-adj model in combination with either the AV18 or BONN model.

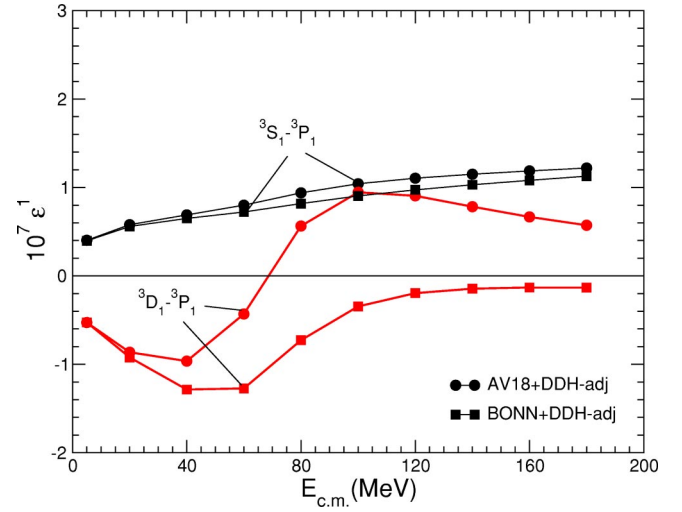


FIG. 9. (Color online) The  ${}^3S_1\text{-}{}^3P_1$  and  ${}^3D_1\text{-}{}^3P_1$  mixing parameters obtained with the DDH-adj model in combination with either the AV18 or BONN model.

culated by retaining in the partial-wave expansion for the amplitude, Eq. (4.26), all channels with  $J$  up to  $J_{\max}=6$ . There is very little sensitivity to the input strong-interaction potential. As also remarked in Ref. [6], this reduced sensitivity is undoubtedly a consequence of the fact that present potentials are fitted to extended  $pp$  and  $pn$  databases with high accuracy.

Figure 12 shows that the total asymmetries obtained by including only the  $J=0$  and 1 channels ( ${}^1S_0\text{-}{}^3P_0$ ,  ${}^3S_1\text{-}{}^3P_1$ ,  ${}^3D_1\text{-}{}^3P_1$ ,  ${}^3S_1\text{-}{}^1P_1$ , and  ${}^3D_1\text{-}{}^1P_1$ ) and, in addition, the  $J=2$  channels, and finally all  $J$  channels up to  $J_{\max}=6$ . In the energy range 0–200 MeV the asymmetry is dominated by the  $J=0\text{-}2$  contributions.

For completeness, we present in Figs. 13 and 14 results for the angular distributions of the (PC) spin-averaged differential cross section and (PV) longitudinal asymmetry at center-of-mass energies of 20 MeV and 100 MeV. The asymmetry  $A(E, \theta)$  is defined in Eq. (5.2).

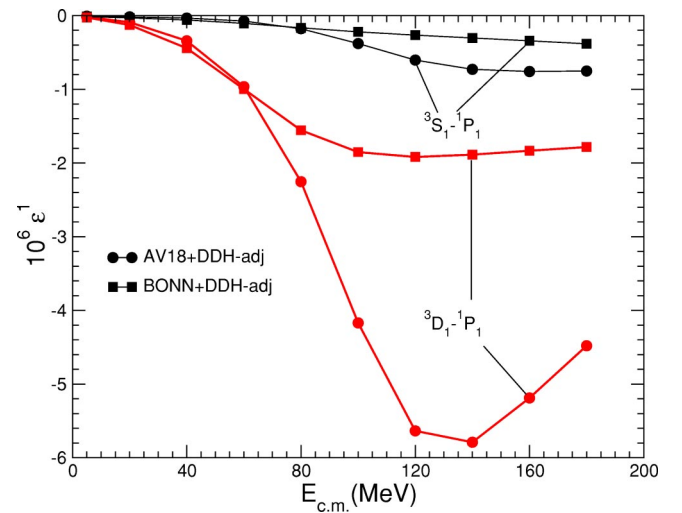


FIG. 10. (Color online) Same as in Fig. 9 but for the  ${}^3S_1\text{-}{}^1P_1$  and  ${}^3D_1\text{-}{}^1P_1$  mixing parameters.

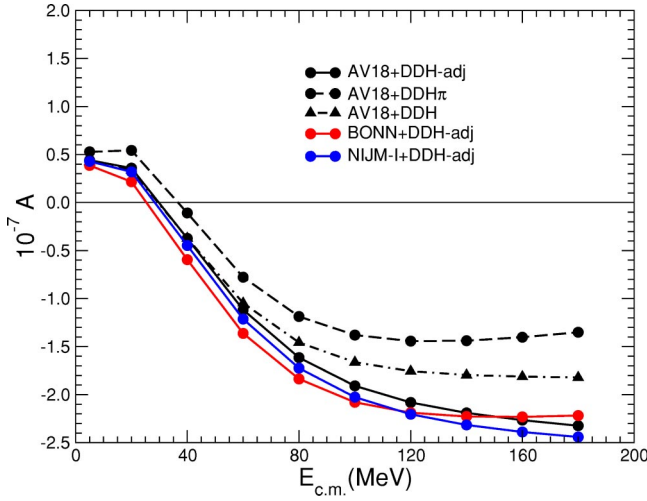


FIG. 11. (Color online) The neutron asymmetry obtained with various combinations of strong- and weak-interaction potentials, as function of the center-of-mass energy.

The predictions for the neutron spin rotation per unit length,  $d\phi/dd$  with  $\phi$  defined in Eq. (5.11), are listed in Table V in the limit of vanishing incident neutron energy. The density of liquid hydrogen is taken as  $\rho=0.4 \times 10^{23}$  = atoms  $\text{cm}^{-3}$ .

While results corresponding to different input strong interactions are within  $\leq 10\%$  of each other, the calculated values show significant sensitivity to the short-range structure of the PV interaction, columns labeled DDH-adj and DDH. It is worth reemphasizing that the longitudinal asymmetry in  $\bar{p}p$  elastic scattering predicted by the DDH model is at variance with that observed experimentally [6]. The short-range cutoff parameters and combinations of  $\rho$ - and  $\omega$ -meson PV coupling constants in  $TT_z=11$ , respectively  $h_\rho^0+h_\rho^1+h_\rho^2/\sqrt{6}$  and  $h_\omega^0+h_\omega^1$ , were constrained, in the DDH-adj model, to re-

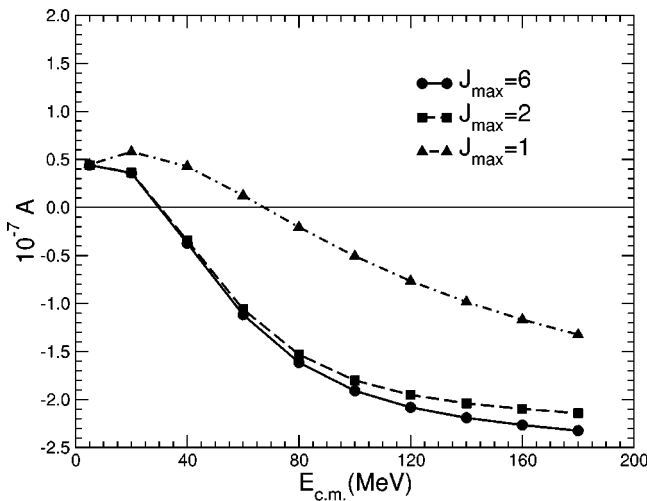


FIG. 12. Contributions to the neutron asymmetry obtained by including only the  $J=0$  and  $J=1$  channels, and by adding the  $J=2$  channels, and finally all  $J$  channels up to  $J_{\max}=6$ . The AV18+DDH-adj potential combination is used; black solid line in Fig. 11.

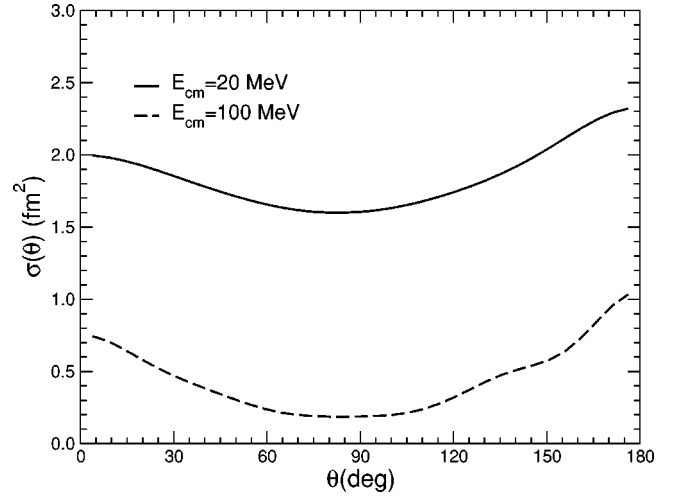


FIG. 13. Angular distributions for the spin-averaged  $np$  (strong-interaction) cross section at center-of-mass energies of 20 MeV and 100 MeV, corresponding to the AV18 potential.

produce this (measured) asymmetry [6]. An additional difference between the DDH-adj and DDH models is in the values adopted for the (PC)  $\rho$ -meson tensor coupling to the nucleon, 6.1 in the DDH-adj (from the BONN interaction) and 3.7 in the DDH (consistent with estimates from vector-meson dominance). Comparison between the DDH-adj and DDH $\pi$  predictions, however, indicates that the neutron-spin rotation is sensitive to the long-range part of  $v^{\text{PV}}$ , and therefore a measurement of this observable would be useful in constraining the PV  $\pi NN$  coupling constant.

Finally, there is a sign difference between the present results and those reported in Ref. [43]. It is not due to the different strong-interaction potential used in that calculation. Indeed, with the Paris potential [51] in combination with the DDH model we obtain  $d\phi/dd=+8.88 \times 10^{-9}$  rad  $\text{cm}^{-1}$ , the same magnitude as but opposite sign from that given in Ref. [43].

In order to understand this discrepancy, we have carried out a calculation of the neutron-spin rotation, which ignores

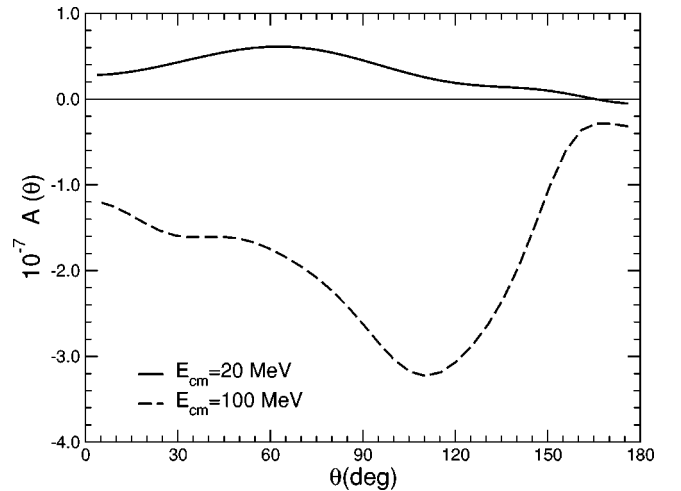


FIG. 14. Angular distributions for the neutron asymmetry at center-of-mass energies of 20 MeV and 100 MeV. The AV18+DDH-adj potential combination is used; dark solid line in Fig. 11.



TABLE V. Neutron spin-rotation angle per unit length, in units of  $10^{-9}$  rad  $\text{cm}^{-1}$ , in the limit of vanishing incident neutron energy. Various combinations of strong- and weak-interaction potentials are used. Also listed are the results obtained by ignoring strong-interaction effects, row labeled “plane waves.”

	DDH-adj	DDH $\pi$	DDH
AV18	5.09	5.21	7.19
NIJM-I	4.94	5.35	7.64
BONN	4.63	5.18	7.35
Plane waves	-5.67	-6.87	-5.85

strong-interaction effects. It is equivalent to a first-order (in  $v^{\text{PV}}$ ) perturbative estimate of this observable, and the corresponding results, listed in the last row of Table V (row labeled “plane waves”), demonstrate that strong-interaction distortion effects are crucial, in fact they are responsible for flipping the sign of  $\phi$ . This is in contradiction with the statement reported in the first paragraph after Eq. (6) of Ref. [43]: Avishai and Grange claim that the “plane-wave” prediction with the DDH model is  $-6.0 \times 10^{-9}$  rad  $\text{cm}^{-1}$ , namely, it has the same sign as in their full calculation.

The sign difference between the predictions obtained by either including or neglecting strong-interaction distortion effects can easily be understood. For simplicity, consider the DDH $\pi$  model, in which case the relevant matrix element contributing to  $\phi$  is  $\langle {}^3P_1 | v^{\text{PV}}(\text{DDH}\pi) | {}^3S_1 \rangle$ , connecting the continuum  $T=0^3S_1$  and  $T=1^3P_1$  channels. The essential difference between the undistorted and distorted  ${}^3S_1$  wave functions is the presence of a node in the latter, thus ensuring its orthogonality to the deuteron  ${}^3S_1$  component. It is this node that causes the sign flip.

### B. Photon asymmetry in $\vec{n}p$ radiative capture at low energies

The PV asymmetry  $a^\gamma$  in the  ${}^1\text{H}(\vec{n}, \gamma){}^2\text{H}$  reaction at thermal neutron energies is calculated for the AV18, BONN, and NIJM-I interactions. The asymmetry is expected to be constant for low-energy neutrons up to energies well beyond the 1–15 meV averaged in the experiment currently running at the LANSCE facility [52]. Each strong interaction model has associated two-body currents. For the AV18 we consider the currents from the momentum-independent terms—the  $\pi$ - and  $\rho$ -exchange currents from its  $v_6$  part—as well as from the momentum-dependent terms, as reviewed in Sec. III. Further discussion of the AV18 currents is given below. For the BONN and NIJM-I interactions, we retain only the  $\pi$ - and  $\rho$ -exchange currents with cutoff parameters taken from the BONN model ( $\Lambda_\pi=1.72$  GeV and  $\Lambda_\rho=1.31$  GeV), while we neglect contributions from other meson exchanges. In all calculations, however, the currents associated with the  $\Delta$  excitation and  $\omega\pi\gamma$  transition have been included.

The total cross section  $\sigma^\gamma$  is due to the well-known  $M_1$  transition connecting the PC  ${}^1S_0$   $np$  state to the PC deuteron state. The calculated values for each model are given in Table VI, both for one-body (impulse) currents alone and for the one- and two-body currents. In each case the largest two-

TABLE VI. Total cross section  $\sigma^\gamma$  and parity-violating asymmetry  $a^\gamma$  in the  $\vec{n}p$  radiative capture at thermal neutron energies, obtained in various models. The asymmetry is reported for pion-exchange only (DDH $\pi$ ) and full DDH (DDH-adj) interactions.

Interaction	$\sigma^\gamma(\text{mb})$		$a^\gamma \times 10^8$	
	Impulse current	Full current	DDH $\pi$	DDH-adj
AV18	304.6	334.2	-4.98	-4.92
NIJM-I	305.4	332.5	-5.11	-5.02
BONN	306.5	331.6	-4.97	-4.89

body contribution, approximately two-thirds of the total, comes from the currents associated with pion exchange. The total cross section is in good agreement with experimental results, which are variously quoted as 334.2(0.5) mb [53] or 332.6(0.7) mb [54]. It would be possible to adjust, for example, the transition magnetic moment  $\mu_{\gamma N\Delta}$  of the  $\Delta$ -excitation current to precisely fit one of these values, here we simply choose a  $\mu_{\gamma N\Delta}$  of  $3\mu_N$ , which is consistent with an analysis of  $\gamma$ - $N$  data at resonance.

As discussed in Sec. V B, the PV asymmetry arises from an interference between the  $M_1$  term above and the  $E_1$  transition, connecting the  ${}^3P_1$  PV  $np$  state to the PC deuteron state and the  ${}^3S_1$  PC  $np$  state to the  ${}^3P_1$  PV deuteron state. The  $E_1$  transitions proceeding through the PV  ${}^1P_1$   $np$  or deuteron states are suppressed, because of an isospin selection rule forbidding isoscalar electric-dipole transitions and also because of spin-state orthogonality. In principle, there is a relativistic correction to the electric dipole operator, associated with the definition of the center of energy [46]. However, its contribution in transitions proceeding through the  ${}^1P_1$  channel vanishes too, since the associated operator is diagonal in the pair spin.

The calculated asymmetries are listed in Table VI. The results are consistent with earlier [55,56] and more recent [57,58] estimates, and are in agreement with each other at the few percent level, which is also the magnitude of the contributions from the short-range terms. In particular, they show that this observable is very sensitive to the weak PV  $\pi NN$  coupling constant, while it is essentially unaffected by short-range contributions (in this context, see also Fig. 2). The  $E_1$  transition has been calculated in the long-wavelength approximation (LWA) with the Siegert form of the  $E_1$  operator [see, for example, Eq. (4.5) of Ref. [45]], thus eliminating many of the model dependencies and leaving only simple (long-range) matrix elements. In the notation of Sec. V B, the associated reduced matrix elements are explicitly given by

$$\begin{aligned}
 & E_1({}^3S_1, {}^3S_1) + E_1({}^3D_1, {}^3S_1) \\
 &= i \frac{q}{2\sqrt{6}\pi} \int_0^\infty dr r^2 \left[ u(r; {}^3P_1) \left( w(r; {}^3S_1) - \frac{1}{\sqrt{2}} w(r; {}^3D_1) \right) \right. \\
 & \quad \left. - w(r; {}^3P_1) \left( u(r; {}^3S_1) - \frac{1}{\sqrt{2}} u(r; {}^3D_1) \right) \right], \quad (7.1)
 \end{aligned}$$

TABLE VII. Cumulative contributions (in units of  $10^{-8}$ ) to the PV asymmetry  $a^\gamma$  in the  $\vec{n}p$  radiative capture at thermal neutron energies for the AV18 interaction and pion-exchange-only DDH $\pi$  interaction. See text for explanation.

AV18 (PC) currents	DDH $\pi$ (PV) currents	
Impulse	-15.3	
+ $\pi$	-48.3	44.2
+ $\rho$	-40.4	44.0
+ $p$ dependent	-43.8	44.0

where the  $w$ 's and  $u$ 's denote the  $np$  continuum and deuteron radial wave functions defined, respectively, as in Secs. IV A and IV D (only the outgoing-channel quantum numbers are displayed for the  $w$ 's). Corrections beyond the LWA terms in  $E_1$  transitions have been found to be quite small. For completeness, we also give the well-known expression for the  $M_1$  RME, as calculated to leading order in  $q$  and in the limit in which only one-body currents are retained,

$$M_1(^1S_0, ^1S_0) = i \frac{q}{2\sqrt{2}\pi m} (\mu_p - \mu_n) \int_0^\infty dr ru(r; ^3S_1) w(r; ^1S_0), \quad (7.2)$$

where the combination  $\mu_p - \mu_n = 4.706\mu_N$  is the nucleon isovector magnetic moment.

We have also calculated the  $E_1$  contributions with the full current density operator  $\mathbf{j}(\mathbf{x})$ , namely, by evaluating matrix elements of

$$E_{1\lambda} = \frac{1}{q} \int d\mathbf{x} \mathbf{j}(\mathbf{x}) \cdot \nabla \times j_1(qx) \mathbf{Y}_{1\lambda}^{11}(\hat{\mathbf{x}}), \quad (7.3)$$

where  $\mathbf{Y}_{1\lambda}^{11}$  are standard vector spherical harmonics. To the extent that retardation corrections beyond the LWA of the  $E_1$  operator are negligible [45], this should produce identical results *provided* the current is exactly conserved. In order to satisfy current conservation, currents from both the strong (PC) and weak (PV) interactions are required, as discussed in Sec. III. In the following we keep only the  $\pi$ -exchange term in the DDH interaction (with their ‘‘best guess’’ for the weak  $\pi NN$  coupling constant), and use the AV18 strong-interaction model.

As reviewed in Sec. III, the PC two-body currents constructed from the  $v_6$  part of the AV18 interaction (the  $\pi$ - and  $\rho$ -exchange currents) exactly satisfy current conservation with it. The same holds true for the PV  $\pi$ -exchange currents derived from the DDH interaction in Sec. III A. However, the PC two-body currents originating from the isospin- and momentum-dependent terms of the AV18 are strictly not conserved (see below). The associated contributions, while generally quite small, play here a crucial role because of the large cancellation between the (PC)  $v_6$  currents from the AV18 and the (PV)  $\pi$  currents from the DDH. This point is illustrated in Table VII. Note that the PC currents from  $\Delta$  excitation and  $\omega\pi\gamma$  transition are transverse and therefore do not affect the  $E_1$  matrix element. However, they slightly reduce the PV asymmetry, since their contributions increase

the  $M_1$  matrix element by  $\approx 1\%$ . They are not listed in Table VII.

The asymmetry is given by the sum of the two columns in Table VII, namely,  $+0.17 \times 10^{-8}$  (last row). This value should be compared to  $-5.02 \times 10^{-8}$ , obtained with the Siegert form of the  $E_1$  operator for the same interactions (and currents for the  $M_1$  matrix element). As already mentioned, we have explicitly verified that retardation corrections in the  $E_1$  operator are too small to account for the difference. Thus the latter is to be ascribed to the lack of current conservation, originating from the isospin- and momentum-dependent terms of the AV18.

To substantiate this claim, we have carried out a calculation based on a  $v_8$  reduction [59] of the AV18 (denoted as AV8), constrained to reproduce the binding energy of the deuteron and the isoscalar combinations of the  $S$ - and  $P$ -wave phase shifts (note, however, that we do include in the AV8 the electromagnetic terms from the AV18, omitted in Ref. [59]). For the AV8 model, the  $\pi$ - and  $\rho$ -exchange currents from the isospin-dependent central, spin-spin, and tensor interaction components are constructed as for the AV18, and therefore are exactly conserved. However, the currents from the isospin-independent interaction  $v^b(r_{ij})\mathbf{L}\cdot\mathbf{S}$  are derived by minimal substitution,

$$\mathbf{p}_i \rightarrow \mathbf{p}_i - eP_i\mathbf{A}(\mathbf{r}_i), \quad (7.4)$$

where  $e$  and  $\mathbf{A}$  are the electric charge and vector potential, respectively, and  $P_i$  is the proton projection operator. The linear terms in  $\mathbf{A}$  are written as  $-\int d\mathbf{x} \mathbf{j}(\mathbf{x})\cdot\mathbf{A}(\mathbf{x})$ , and the resulting spin-orbit current density—or, rather, its Fourier transform—reads

$$\mathbf{j}_{b,ij}^{\text{PC}}(\mathbf{q}) = \frac{v^b(r_{ij})}{2} (e^{i\mathbf{q}\cdot\mathbf{r}_i} P_i - e^{i\mathbf{q}\cdot\mathbf{r}_j} P_j) \mathbf{S} \times \mathbf{r}_{ij}. \quad (7.5)$$

In the case of the isospin-dependent terms, after symmetrizing  $v^{b\tau}(r)[\mathbf{L}\cdot\mathbf{S}, \tau_i\cdot\tau_j]_+/2$ , one obtains

$$\mathbf{j}_{b\tau,ij}^{\text{PC}}(\mathbf{q}) = \frac{v^{b\tau}(r_{ij})}{2} (e^{i\mathbf{q}\cdot\mathbf{r}_i} Q_j - e^{i\mathbf{q}\cdot\mathbf{r}_j} Q_i) \mathbf{S} \times \mathbf{r}_{ij}, \quad (7.6)$$

where

$$Q_i \equiv \frac{\tau_i\cdot\tau_j + \tau_{z,i}}{2}. \quad (7.7)$$

While minimal substitution ensures that the current is indeed conserved for the isospin-independent interaction, i.e.,

$$\mathbf{q}\cdot\mathbf{j}_{b,ij}^{\text{PC}}(\mathbf{q}) = [v^b(r_{ij})\mathbf{L}\cdot\mathbf{S}, \rho_i(\mathbf{q}) + \rho_j(\mathbf{q})], \quad (7.8)$$

this prescription does not lead to a conserved current for the isospin-dependent one, since the commutator above generates an isovector term of the type

$$i(\tau_i \times \tau_j)_z \frac{v^{b\tau}(r_{ij})}{2} [\mathbf{L}\cdot\mathbf{S}, e^{i\mathbf{q}\cdot\mathbf{r}_i} - e^{i\mathbf{q}\cdot\mathbf{r}_j}]_+. \quad (7.9)$$

Physically, this corresponds to the fact that isospin-dependent interactions are associated with the exchange of charged particles, which an electromagnetic field can couple to. One can enforce current conservation by introducing an

TABLE VIII. Cumulative contributions to the total cross section  $\sigma^\gamma$  and PV asymmetry  $a^\gamma$  in the  $\vec{n}p$  radiative capture at thermal neutron energies for the AV8 and pion-exchange-only DDH $\pi$  interactions. Also listed is the asymmetry obtained with the Siegert form of the  $E_1$  operator. See text for explanation.

	$\sigma^\gamma(\text{mb})$	$a^\gamma \times 10^8$		
		AV8 (PC) currents	DDH $\pi$ (PV) currents	Total
Impulse	226.4	-17.7		-17.7
$+\pi$	239.2	-57.9	51.3	-6.60
$+\rho$	241.7	-50.3	51.1	+0.790
$+\text{SO}$	241.7	-57.0	51.1	-5.89
$+\Delta + \omega\pi\gamma$	247.4	-56.3	50.5	-5.82
Siegert $E_1$				-5.76

additional term [60], which in the case of  $\mathbf{j}_{b\tau,ij}^{\text{PC}}$  is taken as

$$i(\tau_i \times \tau_j)_z \frac{v^{b\tau}(r_{ij})}{2} \left[ \mathbf{L} \cdot \mathbf{S}_{ij} \frac{e^{i\mathbf{q}\cdot\mathbf{r}_i} - e^{i\mathbf{q}\cdot\mathbf{r}_j}}{\mathbf{q} \cdot \mathbf{r}_{ij}} \right]_+ \quad (7.10)$$

The results obtained for the total cross section and PV asymmetry with the AV8 and pion-only DDH interactions and associated (exactly conserved) currents are listed in Table VIII. A few comments are in order. First, the  $M_1$  cross section in impulse approximation is  $\approx 30\%$  smaller than predicted with the AV18 interaction. This is due to the fact that the  $np$  singlet scattering length obtained with the AV8 (truncated) model is  $-19.74$  fm, and so is about 15% smaller in magnitude than its physical value,  $-23.75$  fm, reproduced by the AV18 within less than 0.1% [9].

Second, the enhancement of the  $M_1$  cross section in the impulse approximation due to (PC) two-body currents, 9.3%, is essentially consistent with that predicted with the AV18.

Lastly, the PV asymmetry obtained with the full currents is close to that calculated with the Siegert form of the  $E_1$  operator. The remaining  $\approx 1\%$  difference is due to numerical inaccuracies as well as additional corrections from retardation terms and higher-order multipoles. Both of these effects are included in the full-current calculation. Note the crucial role played by the spin-orbit currents constructed above.

### C. Deuteron threshold disintegration with circularly polarized photons

The photodisintegration cross sections calculated with the AV18 and BONN models from threshold to 20 MeV photon energies are in excellent agreement with data [61–67]; see Fig. 15. The model dependence between the AV18 and BONN results is negligible. In the calculations the final  $np$  states include interaction effects in all channels up to  $J=5$  and spherical Bessel functions for  $J>5$ , as discussed in the next section.

In the energy regime of interest here, the (total) cross section is dominated by the contributions of  $E_1$  transitions connecting the deuteron to the  $np$  triplet  $P$  waves. The Siegert form is used for the  $E_1$  operator. Because of the way the

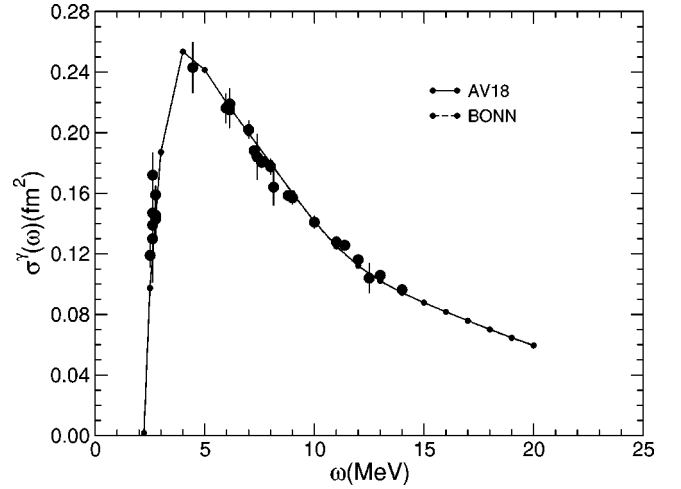


FIG. 15. The deuteron photodisintegration cross sections, calculated with the AV18 and BONN interactions, are compared to data. Note that the AV18 and BONN results are indistinguishable.

calculations are carried out (see Sec. VI), it is conveniently implemented by making use of the following identity for the current density operator  $\mathbf{j}(\mathbf{x})$ , or rather its Fourier transform  $\mathbf{j}(\mathbf{q})$ :

$$\begin{aligned} \mathbf{j}(\mathbf{q}) &= \mathbf{j}(\mathbf{q}) - \mathbf{j}(\mathbf{q}=0) - \int d\mathbf{x} \mathbf{x} \nabla \cdot \mathbf{j}(\mathbf{x}) \\ &= \mathbf{j}(\mathbf{q}) - \mathbf{j}(\mathbf{q}=0) + i \left[ H, \int d\mathbf{x} \mathbf{x} \rho(\mathbf{x}) \right], \end{aligned} \quad (7.11)$$

where in the first line the volume integral of  $\mathbf{j}(\mathbf{x})$  has been reexpressed in terms of the divergence of the current, ignoring vanishing surface contributions, and in the second line use has been made of the continuity equation. Here  $\rho(\mathbf{x})$  is the charge density operator. In evaluating the matrix elements in Eq. (5.26) the commutator term reduces to

$$i \int d\mathbf{x} \mathbf{x} [H, \rho(\mathbf{x})] \rightarrow iq \int d\mathbf{x} \mathbf{x} \rho(\mathbf{x}) \approx iq \sum_i P_i \mathbf{r}_i, \quad (7.12)$$

where  $P_i$  is the proton projection operator introduced earlier, and relativistic corrections to  $\rho(\mathbf{x})$ , such as those associated with spin-orbit and pion-exchange contributions [45,46], have been neglected.

We have also calculated the photodisintegration cross section by using the expression given in Eq. (7.3) for the  $E_1$  operator, or equivalently by calculating matrix elements of the current  $\mathbf{j}(\mathbf{q})$  without resorting to the identity in Eq. (7.11). The results obtained by including only the one-body terms and both the one- and two-body terms in  $\mathbf{j}(\mathbf{q})$  are compared with those obtained in the Siegert-based calculation (as well as with data) in Fig. 16. The same conclusions as in the previous section remain valid here. Had the current been exactly conserved, then the Siegert-based and full  $\mathbf{j}(\mathbf{q})$  calculations would have produced identical results. The small differences in the case of the AV18 model, as an example, are to be ascribed to missing isovector currents associated with

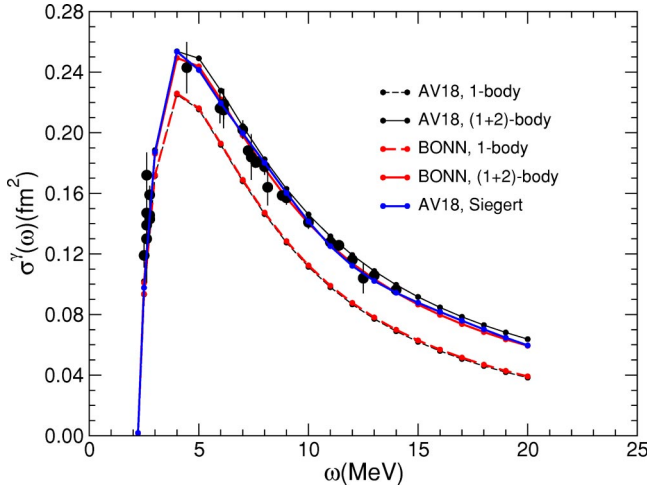


FIG. 16. (Color online) The deuteron photodisintegration cross sections, calculated with the AV18 and BONN interactions, are compared to data. Results obtained by including only one-body terms and both one- and two-body terms in the electromagnetic current are shown along with those calculated by using the right-hand side of Eq. (7.11). The latter are the same as in Fig. 15.

its momentum-dependent interaction components (see previous section).

The PV photon polarization parameter  $P^\gamma$ , obtained with various combinations of PC and PV interactions, is displayed in Fig. 17, while its value at a photon energy  $\approx 1.3$  keV above breakup threshold is listed in Table IX. All results presented below use the current operator in the form given on the right-hand side of Eq. (7.11). Note that, as discussed in Sec. V C, the parameters  $P^\gamma$  for the direct  $d(\vec{\gamma}, n)p$  and inverse  $p(n, \vec{\gamma})d$  processes are the same. In the threshold region, a few keV above breakup, the expression for  $P^\gamma$  reduces to

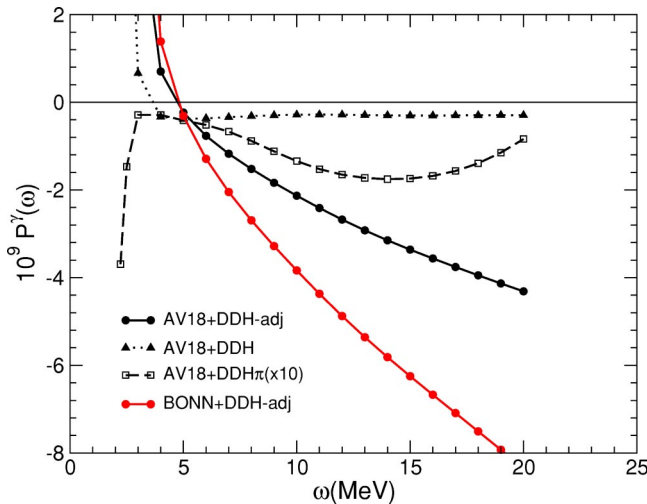


FIG. 17. (Color online) The photon helicity-dependent asymmetries obtained with various combinations of strong- and weak-interaction potentials. Note that the predictions corresponding to the AV18+DDH $\pi$  potential combination are suppressed by roughly one order of magnitude relative to those corresponding to the AV18+DDH-adj and AV18+DDH models. All results are obtained by using the right-hand side of Eq. (7.11).

TABLE IX. Photon helicity-dependent asymmetries (in units of  $10^{-8}$ ) calculated with various combinations of strong- and weak-interaction potentials at an incident photon energy of 2.2259 MeV, about 1.3 keV above threshold. Predictions are listed obtained by including only one-body terms (impulse) and both one- and two-body terms (full) in the electromagnetic current, right-hand side of Eq. (7.11).

	AV18(BONN)+DDH-adj	AV18+DDH $\pi$	AV18+DDH
Impulse	5.44 (9.41)	-0.035	2.49
Full	5.19 (9.05)	-0.037	2.38

$$P^\gamma = \frac{2 \operatorname{Re}[M_1(^1S_0)E_1(^1S_0)]}{|M_1(^1S_0)|^2}, \quad (7.13)$$

where, in the notation of the previous section, the  $M_1(^1S_0)$  RME is defined as in Eq. (5.23) and similarly for  $E_1(^1S_0)$ . In this energy region, the only relevant channel in the final  $np$  state has  $J=0$ ; see the discussion at the end of Sec. V B. Note that the combination of RMEs occurring in  $P^\gamma$  is different from that in  $a^\gamma$ , the photon angular asymmetry parameter measured in  $\bar{n}p$  radiative capture. Indeed, in contrast to  $a^\gamma$ , the photon polarization parameter is almost entirely determined by the short-range part of the DDH interaction, mediated by vector-meson exchanges (and having isoscalar and isotensor character [68]); see Table IX and Fig. 17. This is easily understood, since in the  $^1S_0$ - $^3P_0$  channel the pion-exchange component of the DDH interaction vanishes. Furthermore, the  $E_1$  transition connecting the  $^1S_0$   $np$  continuum state to the PV  $^3P_1$  component of the deuteron, which is predominantly induced by the pion-exchange interaction, is strongly suppressed, to leading order, by spin-state orthogonality. Higher-order corrections, associated with retardation effects and relativistic contributions to the electric dipole operator, were estimated in Ref. [69] and were found to be of the order of a few percent of the leading result arising from vector-meson exchanges. Some of these corrections are retained in the present study.

The predictions in Table IX and in Fig. 17 display great sensitivity both to the strengths of the PV vector-meson couplings to the nucleon and to differences in the short-range structure of the strong-interaction potentials, thus reinforcing the conclusion that these short-ranged meson couplings are not in themselves physical observables; rather, the parity-violating mixings are the physically relevant parameters [70].

Note that the  $\approx 5\%$  decrease in  $P^\gamma$  values between the rows labeled “impulse” and “full” is due to the corresponding 5% enhancement of the  $M_1$  transition connecting the PC  $^1S_0$  and deuteron states, due to two-body terms in the electromagnetic current included in the “full” calculation.

The results in Table IX are consistent in both sign and order of magnitude with those of earlier studies [71–74]; remaining numerical differences are to be ascribed to different strong- and weak-interaction potentials adopted in these earlier works. Indeed, we have explicitly verified that by using the PC AV18 potential and the Cabibbo model for the

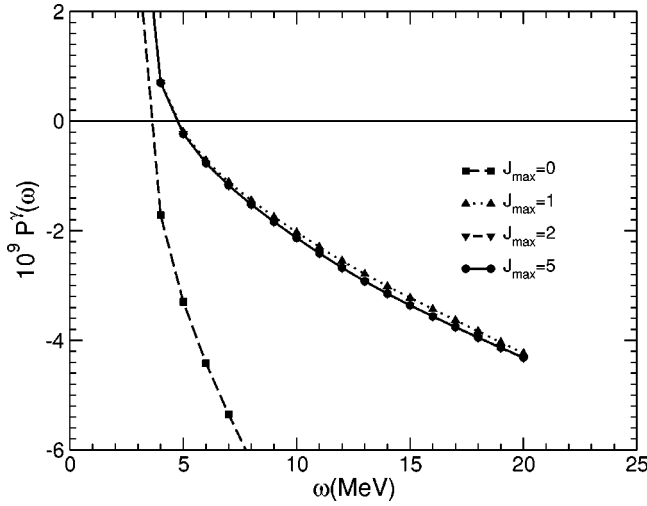


FIG. 18. Contributions to the photon helicity-dependent asymmetry obtained by including PV admixtures in the wave functions of all channels up to  $J_{\max}$ , with  $J_{\max}=0, 1, 2$ , and  $5$ . The AV18+DDH-adj potential combination is used; black solid line in Fig. 17. Note that the curves labeled  $J=2$  and  $J=5$  are indistinguishable.

PV potential [75] we obtain  $P^\gamma$  values close to those reported in Refs. [73,74]. However, our results seem to be at variance with those of Ref. [76] at photon energies a few MeV above the breakup threshold. In particular, Table II in that paper suggests that at 10 and 20 MeV the dominant contribution to  $P^\gamma$  is from the PV pion-exchange interaction and that  $P^\gamma$  has the values  $-2.66 \times 10^{-8}$  and  $-4.54 \times 10^{-8}$ , respectively. This is in contrast to what reported in Fig. 17 of the present work, curves labeled AV18+DDH and AV18+DDH $\pi$ . There is a two orders of magnitude difference between the values referred to above and those obtained here. These differences have been discussed in several recent publications [77–79]. Some of them might be due to the use, in Oka’s work (Ref. [76]), of the “old” Hamada-Johnston potential [80] to generate the PC wave functions, and also to his omission of a contribution associated with a transition connecting the PV admixture to the  $^3P_1$  state and the deuteron, as pointed out by the authors of Ref. [79].

The results in Table IX are consistent with the latest experimental determination,  $P^\gamma=(1.8 \pm 1.8) \times 10^{-7}$  [81], but about two orders of magnitude smaller than an earlier measurement [82].

Figure 18 shows the photon-polarization parameter obtained by including PV admixtures in the  $np$  continuum wave functions of all channels with  $J \leq J_{\max}$  and  $J_{\max}=0, 1, 2$ , and  $5$ . In the energy range explored so far,  $P_\gamma$  is essentially given by the contributions of the  $J=0$  and  $1$  channels.

Finally, Fig. 19 illustrates the effects of two-body terms in the electromagnetic current, written as in the right-hand side of Eq. (7.11). The associated contributions are of the order of a few percent relative to those from one-body terms.

#### D. Deuteron electrodisintegration at quasielastic kinematics

In this section we present results for the asymmetries  $A_{\gamma\gamma}$  and  $A_{\gamma Z}$  obtained by including one- and two-body terms in

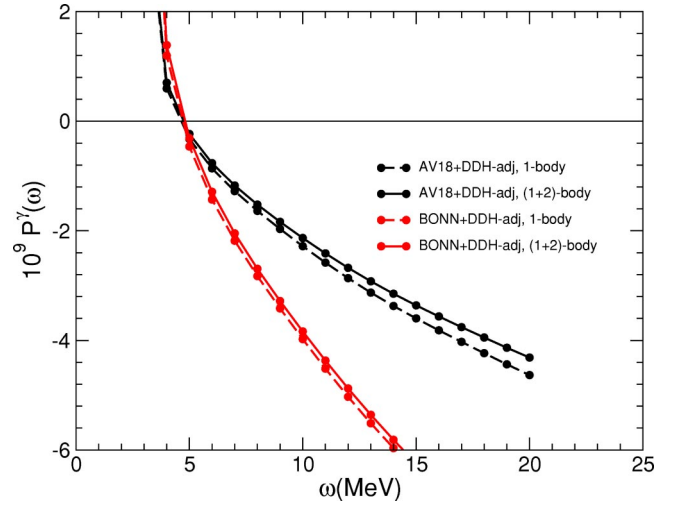


FIG. 19. (Color online) The photon helicity-dependent asymmetries obtained with the AV18+DDH-adj and BONN+DDH-adj potential combinations by including only one-body terms and both one- and two-body terms in the right-hand side of Eq. (7.11).

the electromagnetic and neutral weak currents. Note, however, that only the PV two-body terms associated with  $\pi$  exchange in the DDH interaction are considered in the present calculations (in addition, of course, to the PC terms discussed in Sec. III). The PV currents from  $\rho$  and  $\omega$  exchange have been neglected, since they are expected to play a minor role due to their short-range character. One should also observe that at the higher momentum transfers of interest here, 100–300 MeV/ $c$ , relevant for the SAMPLE experiments [4,83], it is not possible to include the contributions of electric multipole operators through the Siegert theorem; these must be calculated explicitly from the full current.

The  $A_{\gamma Z}$  contribution was recently studied in Ref. [32], where it was shown that two-body terms in the nuclear electromagnetic and weak neutral currents only produce (1–2)% corrections to the asymmetry due to the corresponding single-nucleon currents. The present study—a short account of which has been published in Ref. [7]—investigates the asymmetry originating from hadronic weak interactions. It updates and sharpens earlier predictions obtained in Refs. [84,85]—for example, these calculations did not include the effects of two-body currents induced by PV interactions.

The present calculation proceeds as discussed in Sec. VI. We have used the AV18 or BONN model (and associated currents) in combination with the full DDH interaction (with coupling and cutoff values as given in Table I). The final state, labeled by the relative momentum  $\mathbf{p}$ , pair spin and  $z$  projection  $SM_S$ , and pair isospin  $T$  ( $M_T=0$ ), is expanded in partial waves; PC and PV interaction effects are retained in all partial waves with  $J \leq 5$ , while spherical Bessel functions are employed for  $J > 5$ . In the quasielastic regime of interest here, it has been found that interaction effects are negligible for  $J > 5$ .

In Figs. 20 and 21 we show, respectively, the inclusive cross section and the asymmetries  $A_{\gamma Z}$  and  $A_{\gamma\gamma}$  obtained with the AV18 and DDH-adj interactions, for one of the two SAMPLE kinematics, corresponding to a three-momentum

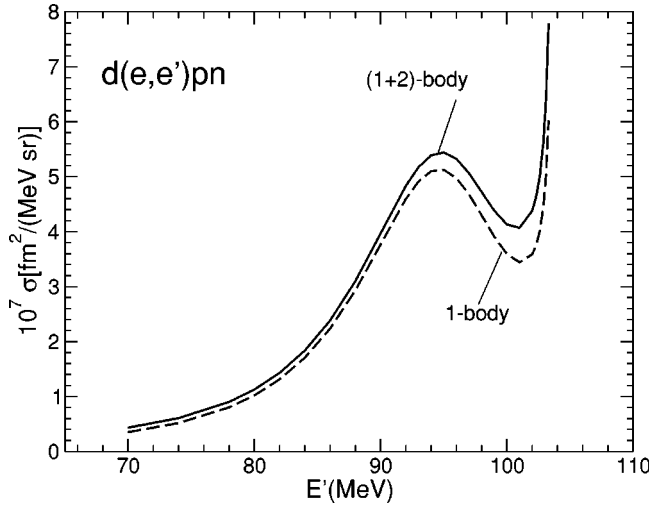


FIG. 20. The  $d(e, e')np$  inclusive cross section calculated, as function of the scattered electron energy  $E'$ , with the AV18 interaction model. The electron incident energy is 117 MeV and its scattering angle  $\theta_e$  is  $138.4^\circ$ . Predictions are shown obtained with one-body terms alone and both one- and two-body terms in the electromagnetic current.

transfer range between 176 MeV and 206 MeV at the low and high ends of the spectrum in the scattered electron energy  $E'$ ; the four-momentum transfer  $|q_\mu^2|$  at the top of the quasielastic peak is  $\approx 0.039 \text{ GeV}^2$ . The rise in the cross section at the high end of the  $E'$  spectrum—the threshold region—is due to the  $M_1$  transition connecting the deuteron to the (quasibound)  $np \ ^1S_0$  state. Note that, because of the well-known destructive interference between the one-body current contributions originating from the deuteron  $S$ - and  $D$ -wave components, two-body current contributions are relatively large in this threshold region. However, they only

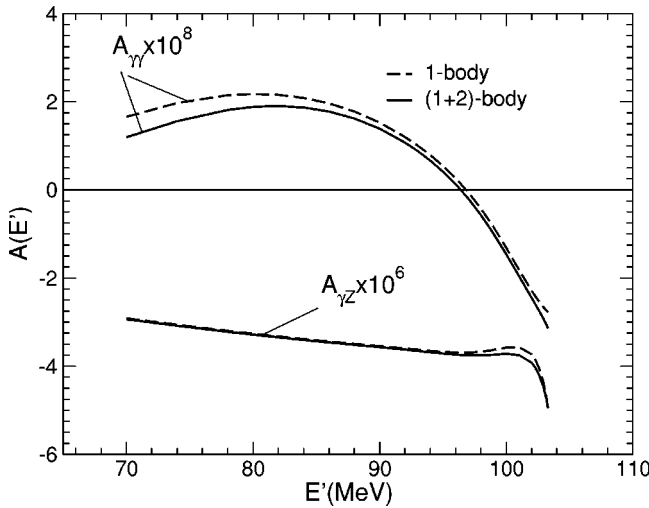


FIG. 21. The asymmetries  $A_{\gamma\gamma}$  and  $A_{\gamma Z}$  calculated, as function of the scattered electron energy  $E'$ , with the (PC) AV18 and (PV) DDH-adj interaction models. The other electron kinematical variables are as in Fig. 20. Predictions are shown obtained with one-body terms alone and both one- and two-body terms in the electromagnetic and neutral weak currents.

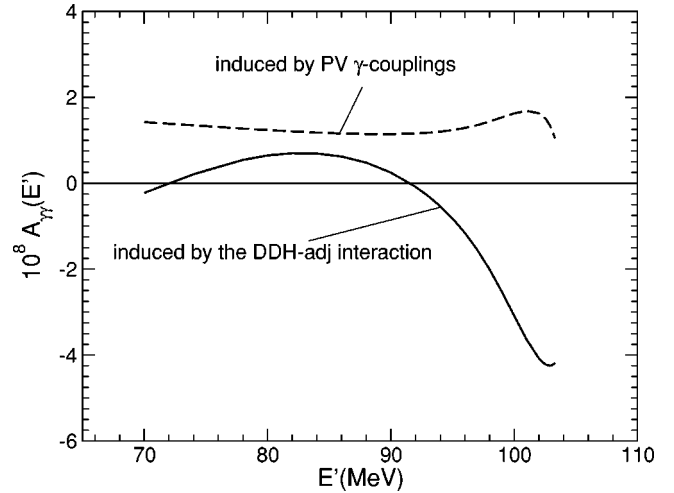


FIG. 22. Contributions to the asymmetry  $A_{\gamma\gamma}$  calculated, as function of the scattered electron energy  $E'$ , with the (PC) AV18 and (PV) DDH-adj interaction models. The other electron kinematical variables are as in Fig. 20. The solid line represents the results corresponding to the presence in the wave functions of opposite-parity components induced by the DDH interaction, while the dashed line represents the results due to the anapole current and the PV two-body current associated with  $\pi$  exchange. The total asymmetry  $A_{\gamma\gamma}$  shown by the solid line in Fig. 21 is obtained as the sum of these two contributions.

amount to a  $\approx 5\%$  correction in the quasielastic peak region.

In Fig. 21 the asymmetry  $A_{\gamma Z}$  labeled (1+2)-body— $A_{\gamma Z}$  is defined in Eq. (5.42)—includes, in addition to one-body, two-body terms in the electromagnetic and neutral weak currents (in both the vector and axial-vector components of the latter). These two-body contributions are negligible over the whole  $E'$  spectrum. However, the (PC and PV) two-body electromagnetic currents play a relatively more significant role in the asymmetry  $A_{\gamma\gamma}$  Eq. (5.41).

In Fig. 22 we display separately, for the asymmetry  $A_{\gamma\gamma}$  the contributions originating from (i) the presence in the wave functions of opposite-parity components induced by the DDH-adj interaction (solid curve) and (ii) the anapole current and the PV two-body current associated with  $\pi$  exchange (dashed curve). The latter are positive and fairly constant as function of  $E'$ , while the former exhibit a pronounced dependence upon  $E'$ . Note that, up to linear terms in the effects induced by PV interactions, the asymmetry  $A_{\gamma\gamma}$  is obtained as the sum of these two contributions.

The BONN model leads to predictions for the inclusive cross section and asymmetries that are very close to those obtained with the AV18, as shown for  $A_{\gamma Z}$  and  $A_{\gamma\gamma}$  in Fig. 23. Thus the strong-interaction model dependence is negligible for these observables.

In Fig. 24 we present results for the asymmetries corresponding to a four-momentum transfer  $|q_\mu^2|$  at the top of the quasielastic peak of about  $0.094 \text{ GeV}^2$ ; the three-momentum transfer values span the range (266–327) MeV over the  $E'$  spectrum shown. The calculations are based on the AV18 model and include one- and two-body currents. The asymmetry from  $\gamma$ - $Z$  interference scales with  $q_\mu^2$  and therefore is, in magnitude, about a factor of 2 larger than calculated in

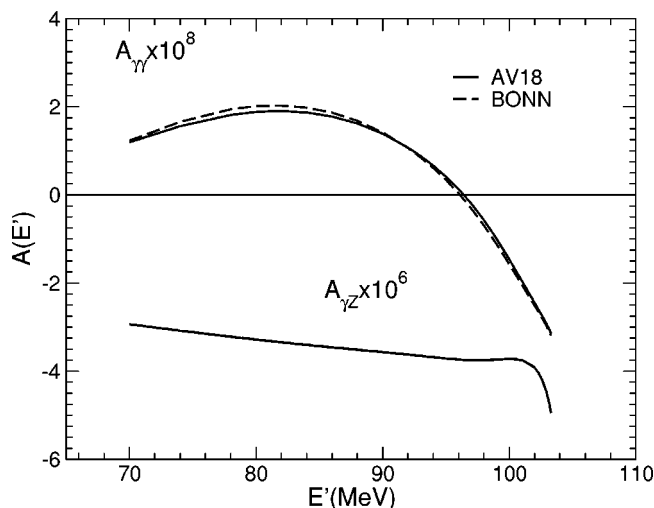


FIG. 23. The asymmetries  $A_{\gamma\gamma}$  and  $A_{\gamma Z}$  calculated, as function of the scattered electron energy  $E'$ , with the DDH-adj model in combination with either the AV18 or BONN model. The other electron kinematical variables are as in Fig. 20. Predictions are shown obtained by including one- and two-body terms in the electromagnetic and neutral weak currents. For the  $A_{\gamma Z}$  asymmetry the AV18 and BONN calculated values are essentially indistinguishable.

Fig. 21 where  $|q_{\mu}^2| \approx 0.039 \text{ GeV}^2$ . The contributions to  $A_{\gamma\gamma}$  exhibit, as functions of  $E'$ , a behavior qualitatively similar to that obtained at the lower  $|q_{\mu}^2|$  value; see Fig. 22.

In Fig. 25 we compare results for the contribution to  $A_{\gamma\gamma}$  due to the presence in the wave function of opposite-parity components induced by the full DDH-adj and a truncated version of it, including only the pion-exchange term. Note that, up to linear terms in the effects produced by PV interactions, the other contribution to  $A_{\gamma\gamma}$ , namely, that originat-

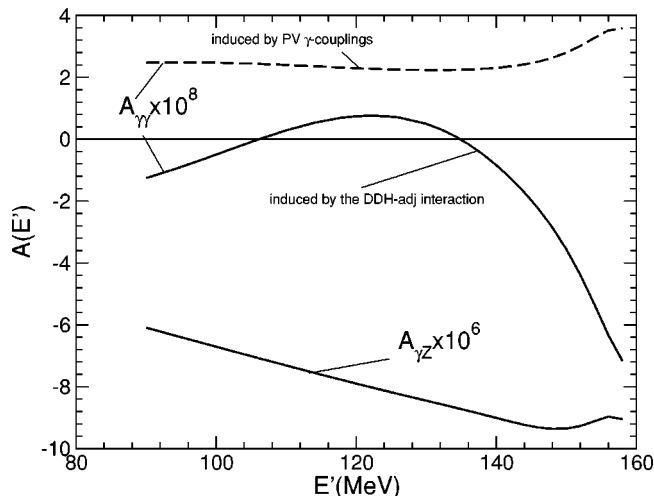


FIG. 24. The asymmetry  $A_{\gamma Z}$  and the two contributions to the asymmetry  $A_{\gamma\gamma}$  (notation as in Fig. 22) calculated, as function of the scattered electron energy  $E'$ , with the (PC) AV18 and (PV) DDH-adj interaction models. Predictions are shown obtained by including one- and two-body terms in the electromagnetic and neutral weak currents. Note that the electron incident energy is 192 MeV and its scattering angle  $\theta_e$  is  $138.4^\circ$ .

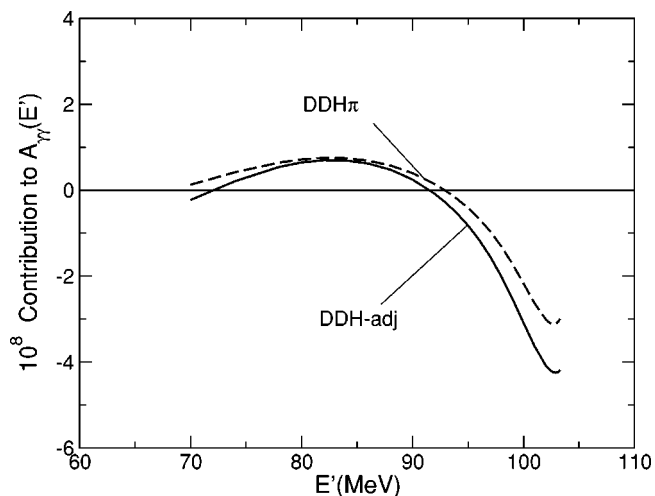


FIG. 25. Contribution to the asymmetry  $A_{\gamma\gamma}$ , calculated as function of the scattered electron energy  $E'$ , corresponding to the presence in the wave functions of opposite-parity components induced by either the full DDH-adj or a truncated DDH model, consisting of its pion-exchange component only, in combination with the AV18 model. The other electron kinematical variables are as in Fig. 20. Predictions are shown obtained by including (PC and PV) one- and two-body terms in the electromagnetic current.

ing from (PV) one- and two-body currents, remains the same as in Fig. 22, since—as mentioned earlier—only the (PV) two-body currents associated with pion exchange are considered in the present work. Figure 25 shows that the asymmetry  $A_{\gamma\gamma}$  is dominated by the long-range pion-exchange contribution. Hence,  $A_{\gamma\gamma}$  will scale essentially linearly with the PV  $\pi NN$  coupling constant.

Finally, Fig. 26 is meant to illustrate the sensitivity of the asymmetry  $A_{\gamma\gamma}$  to those PC two-body currents derived from the momentum-dependent interaction components of the AV18 model (i.e., the spin-orbit,  $L^2$ , and quadratic-spin-orbit terms); see Secs. III and VII B. While these currents play a crucial role in the photon asymmetry in the  $\vec{n}\vec{p}$  radiative capture at thermal neutron energy, they give negligible contributions to the present observable at quasielastic kinematics.

These results demonstrate that, in the kinematics of the SAMPLE experiments [4,83], the asymmetry from  $\gamma$ -Z interference is dominated by one-body currents, and that it is two orders of magnitude larger than that associated with the PV hadronic weak interaction. Hence even the largest estimates of the weak  $\pi NN$  coupling constant will not affect extractions of single-nucleon matrix elements. These conclusions corroborate those of the authors of Ref. [86], who have carried out a similar study of the impact of hadronic weak interaction on quasielastic electrodeuteron scattering.

## VIII. CONCLUSIONS

A systematic study of parity-violating observables in the  $np$  system, including the asymmetries in  $\vec{n}\vec{p}$  radiative capture and  $d(\vec{\gamma}, n)p$  photodisintegration, the spin rotation and longitudinal asymmetry in  $\vec{n}\vec{p}$  elastic scattering, and the asymmetry in electrodisintegration of the deuteron by polarized elec-

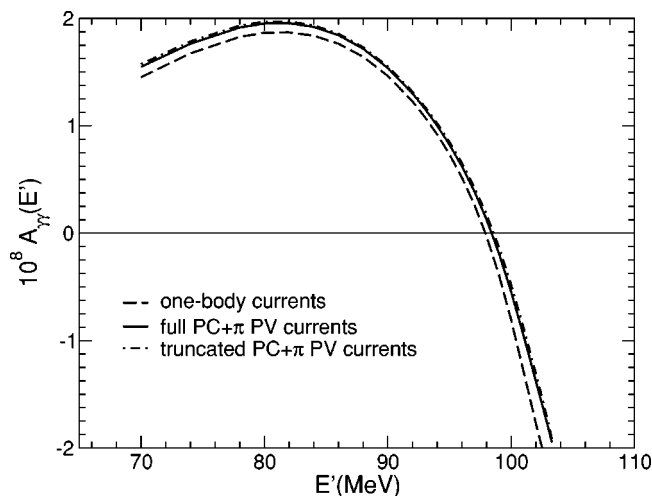


FIG. 26. The asymmetry  $A_{\gamma\gamma}$  calculated, as function of the scattered electron energy  $E'$ , with the AV18 model in combination with a truncated DDH model consisting of its pion-exchange component only. The other electron kinematical variables are as in Fig. 20. Predictions are shown obtained by including the one-body terms alone and both the one- and two-body terms in the PC and PV components of the electromagnetic current (dashed and solid lines, respectively). Also shown are the results obtained by ignoring in the PC two-body currents those terms from the momentum-dependent components of the AV18 model (dash-dotted line).

trons at quasielastic kinematics, has been carried out by using a variety of latest-generation, strong-interaction potentials in combination with the DDH model of the PV hadronic weak interaction. We find that the model dependence of the  $\vec{n}p$ -capture asymmetry upon the strong-interaction potential is quite small, at a level similar to the expected contributions of the short-range parts of the interaction. This process is in fact dominated by the long-range interaction components associated with pion exchange. A measurement of the  $\vec{n}p$ -capture asymmetry is then a clean probe of that physics.

Similarly, we find that the asymmetry in the  $d(\vec{e}, e')np$  reaction at quasielastic kinematics is a very clean probe of the electroweak properties of individual nucleons. The processes associated with two nucleons, including PV admixtures in the deuteron and scattering wave functions and electromagnetic two-body currents induced by hadronic weak

interactions, play a very small role at the values of momentum transfers explored so far [4,83].

We also find that the neutron-spin rotation is sensitive to both the pion and vector-meson PV couplings to the nucleon, while exhibiting a modest model dependence, at the level of (5–10)%, due to the input strong-interaction potential adopted in the calculation. Thus a measurement of this observable [87], when combined with measurements of the asymmetries in  $\vec{n}p$  radiative capture [2] and  $\vec{p}p$  elastic scattering [1], could provide useful constraints for some of these PV amplitudes.

The asymmetry in the deuteron disintegration by circularly polarized photons from threshold up to 20 MeV energies is dominated by the short-range components of the DDH interaction. However, it also displays enhanced sensitivity to the short-range behavior in the strong-interaction potentials. Indeed, predictions for the asymmetry at threshold differ by almost a factor of 2, depending on whether the Argonne  $v_{18}$  or Bonn 2000 interaction is used in the calculations. Therefore, this observable cannot provide an unambiguous value of short-range weak meson-nucleon couplings; however, it would be valuable in placing constraints on the hadronic weak mixing angles.

Finally, the issue of electromagnetic current conservation in the presence of parity-conserving and PV potentials has been carefully investigated. In particular, in the case of the  $p(\vec{n}, \gamma)d$  and  $d(\vec{\gamma}, n)p$  processes dramatic cancellations occur between the contributions associated with the two-body currents induced, respectively, by the PC and PV potentials.

#### ACKNOWLEDGMENTS

The authors wish to thank L. E. Marcucci and M. Viviani for interesting discussions and illuminating correspondence, and G. Hale for making available to them experimental data sets of the deuteron photodisintegration. The work of J.C. and M.P. was supported by the U.S. Department of Energy under Contract No. W-7405-ENG-36, and the work of R.S. was supported by DOE Contract No. DE-AC05-84ER40150 under which the Southeastern Universities Research Association (SURA) operates the Thomas Jefferson National Accelerator Facility. Finally, some of the calculations were made possible by grants of computing time from the National Energy Research Supercomputer Center.

[1] A. R. Berdoz *et al.*, Phys. Rev. Lett. **87**, 272301 (2001).  
 [2] W. M. Snow *et al.*, Nucl. Instrum. Methods Phys. Res. A **440**, 729 (2000).  
 [3] B. Wojtsekhowski and W. T. H. van Oers (spokespersons), JLAB letter-of-intent 00-002.  
 [4] R. Hasty *et al.*, Science **290**, 2117 (2000).  
 [5] D. T. Spayde *et al.*, Phys. Rev. Lett. **84**, 1106 (2000).  
 [6] J. Carlson, R. Schiavilla, V. R. Brown, and B. F. Gibson, Phys. Rev. C **65**, 035502 (2002).  
 [7] R. Schiavilla, J. Carlson, and M. Paris, Phys. Rev. C **67**, 032501 (2003).

[8] B. Desplanques, J. F. Donoghue, and B. R. Holstein, Ann. Phys. (N.Y.) **124**, 449 (1980).  
 [9] R. B. Wiringa, V. G. J. Stoks, and R. Schiavilla, Phys. Rev. C **51**, 38 (1995).  
 [10] V. G. J. Stoks, R. A. M. Klomp, C. P. F. Terheggen, and J. J. de Swart, Phys. Rev. C **49**, 2950 (1994).  
 [11] R. Machleidt, Phys. Rev. C **63**, 024001 (2001).  
 [12] J. R. Bergervoet *et al.*, Phys. Rev. C **41**, 1435 (1990).  
 [13] V. G. J. Stoks, R. A. M. Klomp, M. C. M. Rentmeester, and J. J. de Swart, Phys. Rev. C **48**, 792 (1993).  
 [14] B. v. Przewoski *et al.*, Phys. Rev. C **58**, 1897 (1998).



- [15] M. Viviani, R. Schiavilla, and A. Kievsky, Phys. Rev. C **54**, 534 (1996).
- [16] R. Schiavilla, V. R. Pandharipande, and D. O. Riska, Phys. Rev. C **41**, 309 (1990).
- [17] R. Schiavilla, V. R. Pandharipande, and D. O. Riska, Phys. Rev. C **40**, 2294 (1989).
- [18] R. Schiavilla, R. B. Wiringa, V. R. Pandharipande, and J. Carlson, Phys. Rev. C **45**, 2628 (1992).
- [19] J. Carlson, D. O. Riska, R. Schiavilla, and R. B. Wiringa, Phys. Rev. C **42**, 830 (1990).
- [20] L. E. Marcucci, D. O. Riska, and R. Schiavilla, Phys. Rev. C **58**, 3069 (1998).
- [21] R. Schiavilla and D. O. Riska, Phys. Rev. C **43**, 437 (1991).
- [22] W. C. Haxton, C.-P. Liu, and M. J. Ramsey-Musolf, Phys. Rev. C **65**, 045502 (2002).
- [23] C.-P. Liu, C. H. Hyun, and B. Desplanques, Phys. Rev. C **68**, 045501 (2003).
- [24] W. C. Haxton, E. M. Henley, and M. J. Musolf, Phys. Rev. Lett. **63**, 949 (1989).
- [25] M. J. Musolf and B. R. Holstein, Phys. Rev. D **43**, 2956 (1991).
- [26] D. O. Riska, Nucl. Phys. **A678**, 79 (2000).
- [27] C. M. Maekawa and U. van Kolck, Phys. Lett. B **478**, 73 (2000).
- [28] S. L. Zhu, S. J. Puglia, B. R. Holstein, and M. J. Ramsey-Musolf, Phys. Rev. D **62**, 033008 (2000).
- [29] L. E. Marcucci, R. Schiavilla, M. Viviani, A. Kievsky, S. Rosati, and J. F. Beacom, Phys. Rev. C **63**, 015801 (2000).
- [30] L. E. Marcucci, R. Schiavilla, S. Rosati, A. Kievsky, and M. Viviani, Phys. Rev. C **66**, 054003 (2002).
- [31] M. J. Musolf, T. W. Donnelly, J. Dubach, S. J. Pollock, S. Kowalski, and E. J. Beise, Phys. Rep. **239**, 1 (1994).
- [32] L. Diaconescu, R. Schiavilla, and U. van Kolck, Phys. Rev. C **63**, 044007 (2001).
- [33] T. M. Ito *et al.* (in preparation).
- [34] M. L. Goldberger and K. M. Watson, *Collision Theory* (Wiley, New York, 1964).
- [35] W. Glöckle, *The Quantum Mechanical Few-Body Problem* (Springer, Berlin, 1983).
- [36] J. L. Friar, Ann. Phys. (N.Y.) **104**, 380 (1977).
- [37] A. Amghar and B. Desplanques, Z. Phys. A **344**, 191 (1992); Nucl. Phys. **A585**, 657 (1995).
- [38] J. L. Forest, Phys. Rev. C **61**, 034007 (2000).
- [39] R. Schiavilla, Nucl. Phys. **A689**, 84c (2001).
- [40] E. Fermi, *Nuclear Physics* (University of Chicago Press, Chicago, 1950).
- [41] F. C. Michel, Phys. Rev. **133**, B329 (1964).
- [42] L. Stodolsky, Phys. Lett. **50B**, 352 (1974); **96B**, 127 (1980).
- [43] Y. Avishai and P. Grange, J. Phys. G **10**, L263 (1984).
- [44] A. R. Edmonds, *Angular Momentum in Quantum Mechanics* (Princeton University Press, Princeton, NJ, 1957).
- [45] M. Viviani, A. Kievsky, L. E. Marcucci, S. Rosati, and R. Schiavilla, Phys. Rev. C **61**, 064001 (2000).
- [46] K. M. Nollett, R. B. Wiringa, and R. Schiavilla, Phys. Rev. C **63**, 024003 (2001).
- [47] M. J. Musolf and T. W. Donnelly, Nucl. Phys. **A546**, 509 (1992).
- [48] H. J. Pirner and D. O. Riska, Phys. Lett. **44B**, 151 (1973).
- [49] J. M. Blatt and L. C. Biedenharn, Phys. Rev. **86**, 399 (1952).
- [50] H. P. Stapp, T. J. Ypsilantis, and N. Metropolis, Phys. Rev. **105**, 302 (1957).
- [51] M. Lacombe, B. Loiseau, J.-M. Richard, R. Vinh Mau, P. Pireraud, and R. de Tourel, Phys. Rev. C **21**, 861 (1980).
- [52] D. Bowman (private communication).
- [53] A. E. Cox, S. A. R. Wynchank, and C. H. Collie, Nucl. Phys. **74**, 497 (1965).
- [54] S. F. Mughabghab, M. Divadeenam, and N. E. Holden, *Neutron Cross Sections from Neutron Resonance Parameters and Thermal Cross Sections* (Academic, London, 1981); <http://isotopes.lbl.gov/ngdata/sig.htm>
- [55] B. Desplanques, Nucl. Phys. **A242**, 423 (1975); **A335**, 147 (1980).
- [56] B. H. J. McKellar, Nucl. Phys. **A254**, 147 (1975).
- [57] B. Desplanques, Phys. Lett. B **512**, 305 (2001).
- [58] C. H. Hyun, T.-S. Park, and D.-P. Min, Phys. Lett. B **516**, 321 (2001).
- [59] R. B. Wiringa and S. C. Pieper, Phys. Rev. Lett. **89**, 182501 (2002).
- [60] L. E. Marcucci, A. Kievsky, S. Rosati, R. Schiavilla, and M. Viviani (private communication).
- [61] G. R. Bishop *et al.*, Phys. Rev. **80**, 211 (1950).
- [62] A. H. Snell, E. C. Barker, and R. L. Sternberg, Phys. Rev. **80**, 637 (1950).
- [63] S. A. Colgate, Phys. Rev. **83**, 1262 (1951).
- [64] J. H. Carver *et al.*, Nature (London) **167**, 154 (1951).
- [65] Y. Birenbaum, S. Kahane, and R. Moreh, Phys. Rev. C **32**, 1825 (1985).
- [66] R. Moreh, T. J. Kennett, and W. V. Prestwich, Phys. Rev. C **39**, 1247 (1989).
- [67] A. De Graeve *et al.*, Phys. Rev. C **45**, 860 (1992).
- [68] G. S. Danilov, Phys. Lett. **18**, 40 (1965).
- [69] J. L. Friar and B. H. J. McKellar, Phys. Lett. **123B**, 284 (1983).
- [70] G. S. Danilov, Sov. J. Nucl. Phys. **14**, 443 (1972).
- [71] E. Hadjimichael and E. Fischbach, Phys. Rev. D **3**, 755 (1971).
- [72] K. R. Lassey and B. H. J. McKellar, Phys. Rev. C **11**, 349 (1975); **12**, E721 (1975).
- [73] B. A. Craver, E. Fischbach, Y. E. Kim, and A. Tubis, Phys. Rev. D **13**, 1376 (1976).
- [74] H. C. Lee, Phys. Rev. Lett. **41**, 843 (1978).
- [75] E. M. Henley, Annu. Rev. Nucl. Sci. **19**, 367 (1969).
- [76] T. Oka, Phys. Rev. D **27**, 523 (1983).
- [77] I. B. Khriplovich and R. V. Korkin, Nucl. Phys. **A690**, 610 (2001).
- [78] M. Fujiwara and A. I. Titov, Phys. Rev. C **69**, 065503 (2004).
- [79] C.-P. Liu, C. H. Hyun, and B. Desplanques, Phys. Rev. C **69**, 065502 (2004).
- [80] T. Hamada and I. D. Johnston, Nucl. Phys. **34**, 382 (1962).
- [81] V. A. Knyaz'kov *et al.*, Nucl. Phys. **A417**, 209 (1984).
- [82] V. M. Lobashov *et al.*, Nucl. Phys. **A197**, 241 (1972).
- [83] D. H. Beck and R. D. McKeown, Annu. Rev. Nucl. Part. Sci. **51**, 189 (2001).
- [84] W.-Y. P. Hwang and E. M. Henley, Ann. Phys. (N.Y.) **129**, 47 (1980).
- [85] W.-Y. P. Hwang, E. M. Henley, and G. A. Miller, Ann. Phys. (N.Y.) **137**, 378 (1981).
- [86] C.-P. Liu, G. Prezeau, and M. J. Ramsey-Musolf, Phys. Rev. C **67**, 035502 (2003).
- [87] W. M. Snow (private communication).